

# Contribution of anthropogenic and natural sources to atmospheric methane variability

P. Bousquet<sup>1,2</sup>, P. Ciais<sup>1</sup>, J. B. Miller<sup>3,4</sup>, E. J. Dlugokencky<sup>3</sup>, D. A. Hauglustaine<sup>1</sup>, C. Prigent<sup>5</sup>, G. R. Van der Werf<sup>6</sup>, P. Peylin<sup>7</sup>, E.-G. Brunke<sup>8</sup>, C. Carouge<sup>1</sup>, R. L. Langenfelds<sup>9</sup>, J. Lathière<sup>1</sup>, F. Papa<sup>5,10</sup>, M. Ramonet<sup>1</sup>, M. Schmidt<sup>1</sup>, L. P. Steele<sup>9</sup>, S. C. Tyler<sup>11</sup> & J. White<sup>12</sup>

Methane is an important greenhouse gas, and its atmospheric concentration has nearly tripled since pre-industrial times<sup>1</sup>. The growth rate of atmospheric methane is determined by the balance between surface emissions and photochemical destruction by the hydroxyl radical, the major atmospheric oxidant. Remarkably, this growth rate has decreased<sup>2</sup> markedly since the early 1990s, and the level of methane has remained relatively constant since 1999, leading to a downward revision of its projected influence on global temperatures. Large fluctuations in the growth rate of atmospheric methane are also observed from one year to the next<sup>2</sup>, but their causes remain uncertain<sup>2–13</sup>. Here we quantify the processes that controlled variations in methane emissions between 1984 and 2003 using an inversion model of atmospheric transport and chemistry. Our results indicate that wetland emissions dominated the inter-annual variability of methane sources, whereas fire emissions played a smaller role, except during the 1997–1998 El Niño event. These top-down estimates of changes in wetland and fire emissions are in good agreement with independent estimates based on remote sensing information and biogeochemical models. On longer timescales, our results show that the decrease in atmospheric methane growth during the 1990s was caused by a decline in anthropogenic emissions. Since 1999, however, they indicate that anthropogenic emissions of methane have risen again. The effect of this increase on the growth rate of atmospheric methane has been masked by a coincident decrease in wetland emissions, but atmospheric methane levels may increase in the near future if wetland emissions return to their mean 1990s levels.

The global growth rate of atmospheric methane (CH<sub>4</sub>) decreased from nearly +12 ± 2 p.p.b. yr<sup>-1</sup> in the 1980s to +4 ± 4 p.p.b. yr<sup>-1</sup> in the last decade (all values are means ± s.d.), but with large year-to-year variations<sup>2</sup> (Fig. 1a). A peak in growth rate occurred in 1991 in the tropics, followed by a large and abrupt drop in 1992, which began in the northern regions. The past few years have been marked by two positive growth-rate anomalies in 1997–1998 and in 2002–2003, which seem more pronounced north of 30°N than in the tropics.

To understand better why the growth rate of CH<sub>4</sub> has remained persistently smaller after the early 1990s, we have analysed the regional trends in CH<sub>4</sub> differences between sampling sites in the National Oceanic and Atmospheric Association (NOAA) global cooperative air sampling network<sup>2</sup> and the South Pole site, taken as a reference (Fig. 1b and Supplementary Information). This analysis

suggests that either northern CH<sub>4</sub> emissions have declined persistently since 1992 or that the destruction of CH<sub>4</sub> by the hydroxyl radical (OH) has increased north of 30°N. Several conflicting hypotheses have been proposed to explain interannual and long-term variations in atmospheric CH<sub>4</sub>, focusing on wetland CH<sub>4</sub> emissions<sup>10,13,14</sup>, anthropogenic CH<sub>4</sub> emissions<sup>5</sup>, wild fires<sup>6–9,15</sup>, OH photochemistry<sup>3,4,11</sup> and inter-annual wind changes<sup>12</sup>. Various models have been used, but the contribution of each process has not been disentangled in a coherent framework, except for short periods<sup>6,16</sup>. Our understanding of the current methane budget therefore remains plagued by very large uncertainties.

Atmospheric CH<sub>4</sub> measurements can be linked quantitatively to regional sources and sinks by inverse modelling. For the period 1984–2003, the CH<sub>4</sub> concentration responses to the action of OH sinks and regional surface sources were simulated each month with the three-dimensional chemistry transport model LMDZ-INCA<sup>17</sup>. The model was forced with interannual analysed winds<sup>18</sup> and inter-annually varying OH concentrations<sup>19</sup>. Emissions of CH<sub>4</sub> from different regions of the globe and from distinct processes (see Methods), together with the photochemical sinks, were inferred, and their uncertainties reduced, by matching atmospheric observations within their uncertainties in a bayesian formalism<sup>19</sup>. Clearly, uncertainties in the variations of OH concentrations limit our ability to infer accurately fluctuations in regional CH<sub>4</sub> emissions. The removal of CH<sub>4</sub> by OH nearly balances the sum of all surface sources, making the atmospheric CH<sub>4</sub> budget highly sensitive to OH changes. Thus, we constrained first the interannual variability of OH through a preliminary inversion of methyl chloroform atmospheric observations<sup>19</sup>. Contributions of monthly surface CH<sub>4</sub> sources and pre-optimized monthly OH sinks were then combined to fit optimally monthly averages of CH<sub>4</sub> measurements from a global network of 68 sampling sites. Long-term measurements of the <sup>13</sup>C/<sup>12</sup>C ratio in CH<sub>4</sub> (δ<sup>13</sup>C-CH<sub>4</sub>) were also used as an additional constraint for the partitioning of microbial-, biomass-burning- and fossil-fuel-related CH<sub>4</sub> sources. We performed a control inversion, supplemented by an ensemble of 17 sensitivity inversions (see Methods).

We found that the year-to-year CH<sub>4</sub> regional flux changes (or anomalies) can be more robustly inverted than their mean values, a result similar to CO<sub>2</sub> inversions<sup>20,21</sup>. Indeed, among the different sensitivity inversions, the spread of regional flux anomalies is more than a factor of two smaller than the spread of long-term mean fluxes. In other words, possible biases in the inversions seem to have low interannual variability. To illustrate this point, we tested the impact

<sup>1</sup>Laboratoire des Sciences du Climat et de l'Environnement, IPSL-LSCE, CEA-CNRS-UVSQ, F-91191, France. <sup>2</sup>Université de Versailles Saint Quentin en Yvelines, F-78035, France. <sup>3</sup>NOAA Earth System Research Laboratory, Global Monitoring Division, Boulder, Colorado 80305-3328, USA. <sup>4</sup>Cooperative Institute for Research in Environmental Science, Campus Box 216, University of Colorado, Boulder, Colorado 80309, USA. <sup>5</sup>LERMA, Observatoire de Paris, F-75014, France. <sup>6</sup>Faculty of Earth and Life Sciences, Vrije Universiteit, Amsterdam, The Netherlands. <sup>7</sup>Laboratoire de Biogéochimie Isotopique, LBI, F-78026, France. <sup>8</sup>South African Weather Service, Stellenbosch 7599, South Africa. <sup>9</sup>CSIRO, Marine and Atmospheric Research, Victoria 3195, Australia. <sup>10</sup>NASA-GISS-Columbia University, New York, New York 10025, USA. <sup>11</sup>Earth System Science Department, University of California, Irvine, California 92697, USA. <sup>12</sup>Institute of Arctic and Alpine Research, University of Colorado, Boulder, Colorado 80309, USA.

of adding an additional methane source from plants<sup>22</sup> with an *a priori* value of  $+150 \pm 60 \times 10^{12}$  grams of  $\text{CH}_4$  per year ( $\text{Tg of CH}_4 \text{ yr}^{-1}$ ). The long-term-mean inverted fluxes were strongly affected by this 'intrusion' of this new source, but the atmospheric measurements remained fitted and the global budget was conserved, after a reduction in plant and other source emissions ( $-30\%$ ) within their uncertainties. The sparseness of the tropical network, along with large uncertainties on prior emissions, prevents us from verifying the existence of long-term  $\text{CH}_4$  emissions by plants. Adding plants in the *a priori*  $\text{CH}_4$  sources mix, however, did not alter the inferred anomalies in the 1990s (see Supplementary Information). Given their robustness, the flux anomalies are therefore the primary focus of the following analysis.

We found that fluctuations in wetland emissions are the dominant contribution to interannual variability in surface emissions ( $\pm 12 \text{ Tg of CH}_4 \text{ yr}^{-1}$ ), explaining 70% of the global emission anomalies over the past two decades, as compared with only 15% contributed by biomass burning (Fig. 2). This result disagrees with previous studies suggesting a dominant role of fires<sup>6–9,14</sup>. As an independent check on the inverted wetland variability, we applied a simple wetland flux model (see Supplementary Information) based on ref. 23 and driven by interannually varying climate data<sup>18</sup> and by estimates of remotely sensed changes in flooded areas for the period 1993–2001. There is good agreement in the magnitude of the wetland flux anomalies between the bottom-up and inversion results (normalized standard

deviation (NSD) = 1.1; see Methods), as seen in Fig. 2. The correlation between the two estimates is improved when a 3-month lag is applied to the inversion results ( $r^2 = 0.4$ ,  $P = 0.06$ ). In 1993–2001, wetland emissions in the bottom-up model show a persistent negative trend of  $2.5 \text{ Tg of CH}_4 \text{ yr}^{-1}$ , in response to a marked decrease in flooded area worldwide (at a rate of  $-1.1\% \text{ yr}^{-1}$  for a mean area of  $4.2 \times 10^6 \text{ km}^2$ ), mostly in temperate and tropical Asia and in tropical South America<sup>23</sup>. The inversion infers decreasing wetland emissions after 1993, but with a smaller trend ( $-0.6 \text{ Tg of CH}_4 \text{ yr}^{-1}$ ). Shrinking wetland areas may reflect recurrent dryness observed in the tropics after 1990 (ref. 18), and northward after 1999 (ref. 24).

The inversion attributes global variations in the biomass-burning emissions of the order of  $\pm 3.5 \text{ Tg of CH}_4 \text{ yr}^{-1}$  (Fig. 2). In 1989–2002, these anomalies are in very good agreement with independent estimates<sup>9</sup> derived from remote sensing data after 1996 ( $r^2 = 0.6$ ,  $P = 0.012$ ; NSD = 0.8) and inferred from global  $\text{CO}$  variations before 1996 ( $r^2 = 0.4$ ,  $P = 0.08$ ; NSD = 1.2; see Supplementary Information). Such agreement is remarkable, given that the *a priori* biomass-burning fluxes prescribed to the inversion are constant from year to year. The members of the inversion ensemble that include  $\delta^{13}\text{C-CH}_4$  observations agree best with the magnitude of the bottom-up anomalies<sup>9</sup> (NSD = 1.1). At face value, these 'isotopic' inversions

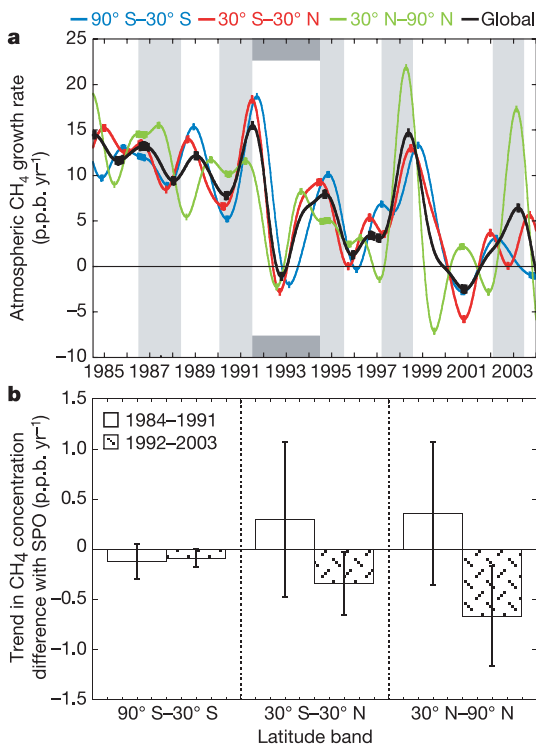


**Figure 1 | Variability and trends in atmospheric  $\text{CH}_4$  over the past two decades.** **a**, Interannual variations in the growth rate of atmospheric  $\text{CH}_4$  ( $\text{p.p.b. yr}^{-1}$ ) in the period 1984–2003, calculated by using data from the NOAA air sampling sites used in the inversion model (maximum of 50 sites). Black, global growth rate; blue, Southern Hemisphere  $<30^\circ\text{S}$ ; red,  $30^\circ\text{S}$  to  $30^\circ\text{N}$  (tropics); green, Northern Hemisphere  $>30^\circ\text{N}$ ; light grey, El Niño episodes; dark grey, anomaly following the Pinatubo climate anomaly. **b**, Average trends in the  $\text{CH}_4$  difference (in  $\text{p.p.b. yr}^{-1}$ ) between sites grouped in three latitude bands and the South Pole site (SPO). Trends were calculated by using monthly deseasonalized observations. Open bars indicate trends in  $\Delta\text{CH}_4$  in the 1980s (1984–1991), when the global growth rate was  $+12 \pm 2 \text{ p.p.b. yr}^{-1}$ ; hatched bars indicate trends in  $\Delta\text{CH}_4$  after 1993, when the global growth rate was  $4 \pm 4 \text{ p.p.b. yr}^{-1}$ . Error bars are 1 s.d. of the calculated trends in differences for the NOAA sites.

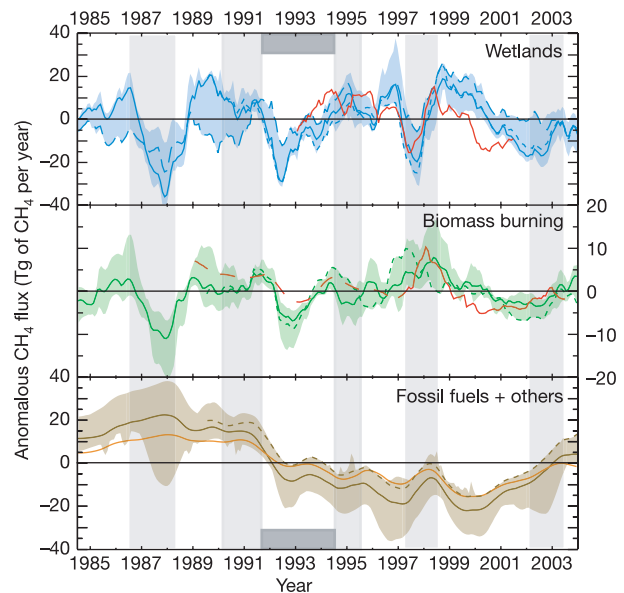


**Figure 2 | Variations in  $\text{CH}_4$  emissions attributed to different processes.** Shown are the interannual global  $\text{CH}_4$  flux anomalies (in  $\text{Tg of CH}_4 \text{ yr}^{-1}$ ; note different y-axis scales) broken down into different processes. Unbroken lines of each sub-panel indicate the member of the ensemble with only  $\text{CH}_4$  observations (control inversion, 68 sites); broken lines of each sub-panel indicate the member of the ensemble with both  $\text{CH}_4$  observations (68 sites) and  $\delta^{13}\text{C-CH}_4$  observations (13 sites after 1998; 4 sites after 1989). Blue indicates wetlands (including rice agriculture); dashed blue line represents wetland anomaly inferred in the extreme case where OH is maintained constant from year to year. Green indicates biomass burning. Brown indicates energy-related sources (fossil fuels, industry, bio-fuels) and other sources (landfills and waste, ruminants, termites, ocean, plants). Unbroken orange line represents the specific contribution of fossil-fuel emissions alone. Red lines indicate set of bottom-up estimates of  $\text{CH}_4$  flux anomalies obtained from a wetland flux model driven by remotely sensed flooded area data<sup>22</sup>, and from a fire model driven by remote sensing measurements after 1997 (ref. 9), and extrapolated using atmospheric carbon monoxide trends before that date (see Supplementary Information). The anomalies are calculated by subtracting the long-term mean  $\text{CH}_4$  flux over the whole period (1984–2003) from the deseasonalized (12-month running mean) monthly flux in each region. Shaded areas represent the spread of an ensemble of 18 inversions (each using *a priori* OH fields pre-optimized from methyl chloroform).

place a strong (tropical) release of CH<sub>4</sub> by fires in 1997, six months earlier than inferred from the remote sensing data (Fig. 2).

The regional patterns of surface CH<sub>4</sub> emissions indicate that most of the global year-to-year variability lies in the tropics (Fig. 3). By contrast, the northern regions show smoother variations, but with systematically less emissions in the 1990s than in the 1980s, except for 1997–1998 and 2002–2003, consistent with Fig. 1b. The variability in CH<sub>4</sub> removal by OH radicals<sup>19</sup> is also dominated by the tropics, where photochemistry remains active all year (Fig. 3). We found that the years 1987–1988, 1991–1992, 1997–1998 and 2001–2002 correspond to abnormally weaker CH<sub>4</sub> destruction by OH in the tropics. In the inversion, a compensation effect exists between the magnitude of methyl-chloroform-derived changes in OH and inverted CH<sub>4</sub> surface emissions, because the sum of the two must equal the observed atmospheric accumulation. Thus, biases in OH changes

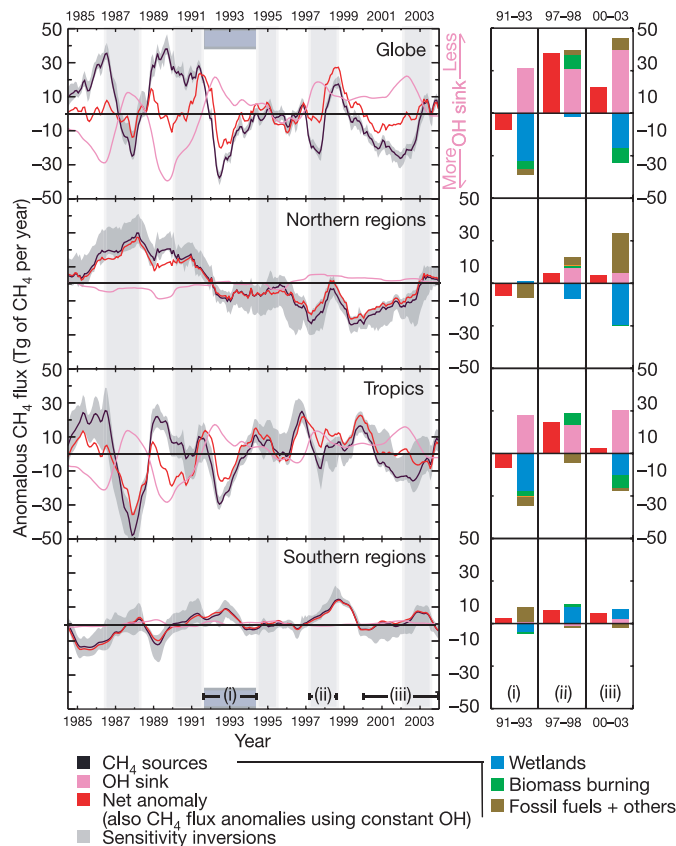


**Figure 3 | Large-scale regional variations in CH<sub>4</sub> emissions and OH sink.** Left, interannual flux anomalies (in Tg of CH<sub>4</sub> yr<sup>-1</sup>) broken down into three large regions<sup>27</sup> for the control inversion: northern regions, tropics and southern regions. Black indicates surface emission anomaly, with grey uncertainty estimates based on the spread of the ensemble of 18 inversions (each using a *a priori* OH variations pre-optimized from methyl chloroform). Pink indicates anomalies in CH<sub>4</sub> removal by OH (negative values mean more CH<sub>4</sub> removal). Red indicates anomalies in the net CH<sub>4</sub> budget in each band; that is, the sum of surface emissions and OH removal. This red line also represents what the surface emissions anomalies would be in the extreme case where OH is maintained constant from year to year. Right, changes in surface emissions and in the OH removal term within each large region during selected remarkable episodes analysed in the text: the drop in CH<sub>4</sub> growth rate of 1991–1993; the high CH<sub>4</sub> growth rate of the 1997–1998 largest El Niño event; and the persistent low mean atmospheric growth rate of 2000–2003. The 1991–1993 anomaly is discussed after subtraction of the mean flux over 1984–2003. The 1997–1998 and the 2000–2003 anomalies are discussed after subtraction of the mean flux over 1993–2003. Quantities refer to the full episode (Tg of CH<sub>4</sub>). A positive bar indicates an increase in surface emission and a decrease in OH removal.

could account for some of the variability that we attributed to wetlands. In the extreme case where OH interannual variability is set at zero, the fluctuations of tropical wetland emissions are dampened by 50%, especially in the 1980s, when methyl chloroform data suggest large OH variability<sup>19</sup>.

We analysed in detail two key perturbations of the CH<sub>4</sub> budget in the past two decades (Fig. 3). First, we studied the drop in growth rate in 1991–1993. This period is particularly intriguing because of the potentially confounding effects of three factors: (1) reduced photochemical production caused by changes in ultraviolet radiation associated with volcanic aerosols emitted in the eruption of the Mount Pinatubo in June 1991; (2) the widespread Northern Hemisphere cooling that followed<sup>25</sup>; and (3) the economic collapse of the former Soviet Union. The first factor should decrease OH, causing CH<sub>4</sub> to increase. Indeed, we inferred a decrease in tropical OH by 5% from the methyl chloroform data<sup>19</sup>, as suggested by Fig. 1b and previous studies<sup>4</sup>. The two other factors should reduce wetland and fossil-fuel emissions respectively, causing atmospheric CH<sub>4</sub> to decrease. Overall, we attribute the 1991–1993 spike in growth rate, a  $-10$  Tg of CH<sub>4</sub> event (Fig. 3), to a large decrease in emissions ( $-36 \pm 6$  Tg of CH<sub>4</sub>) partly offset by a reduction in the OH sink intensity ( $+26$  Tg of CH<sub>4</sub>). Sources that were reduced in that period are predominantly northern and tropical wetlands ( $-24 \pm 6$  Tg of CH<sub>4</sub>) and anthropogenic sources ( $-10 \pm 5$  Tg of CH<sub>4</sub>). Decreased biomass-burning emissions had a much smaller role ( $-5 \pm 2$  Tg of CH<sub>4</sub>). This inversion result agrees well with an independent study showing reduced boreal wetland emissions due to cooler and dryer conditions<sup>10</sup>, and reduced northern anthropogenic emissions<sup>26</sup>.

Second, we investigated the period 1997–1998, which corresponds to the largest El Niño on record. At that time, widespread dryness caused increases of fires in the tropical zone and in boreal regions of Eurasia<sup>9</sup>. In particular, large abnormal peat fires in Indonesia could have released huge amounts of CH<sub>4</sub> to the atmosphere from smouldering combustion<sup>15</sup>. A previous study<sup>9</sup> estimated an anomalous fire source of  $+11.5$  Tg of CH<sub>4</sub> in 1997–1998 (Fig. 3), which agrees well with the inversion estimates ( $+8 \pm 2$  Tg of CH<sub>4</sub> in the tropics and  $+2 \pm 1$  Tg of CH<sub>4</sub> in northern regions). A larger decrease in OH concentration, possibly also caused by large emissions of carbon monoxide<sup>16</sup> and other reactive carbon compounds by fires<sup>7</sup>, is found to contribute to a faster growth of CH<sub>4</sub> by an additional  $+26$  Tg of CH<sub>4</sub>. Natural wetland emissions remained on average stable over the whole 1997–1998 period. However, there was a significant dip in 1997 for the northern regions wetlands ( $-9 \pm 5$  Tg of CH<sub>4</sub>), followed by an increase in 1998 ( $+10 \pm 5$  Tg of CH<sub>4</sub>) in the southern regions (Fig. 3). This shift in regional wetland emissions is fully consistent with the succession of regionally dryer and wetter climate conditions<sup>18</sup>.

Finally, we analysed why the global growth rate of atmospheric CH<sub>4</sub> remained low after the drop in 1991–1993 (ref. 4). After 1993, decreasing global emissions at a rate of  $-1.0 \pm 0.2$  Tg of CH<sub>4</sub> yr<sup>-1</sup> are required to match a small average growth rate of  $+4 \pm 4$  p.p.b. yr<sup>-1</sup>, in the presence of (slightly) decreasing OH (Fig. 3). The inversion attributes this signal to decreasing anthropogenic emissions, in particular to the northern fossil source (Fig. 3). This is in qualitative agreement with the latitudinal CH<sub>4</sub> differences analysed in Fig. 1b. After 1999, however, anthropogenic emissions increase again, especially in north Asia. This may reflect the booming Chinese economy. By 2003, we find that anthropogenic emissions recovered to their levels in the early 1990s. Without a coincident and important drop in northern wetland emissions after 1999 (Fig. 2) associated with dryer conditions<sup>24</sup>, the growth rate of atmospheric CH<sub>4</sub> would therefore have increased much more rapidly. This suggests that the slow-down in CH<sub>4</sub> growth rate observed from the early 1990s may represent only a temporary pause in the human-induced secular increase in atmospheric CH<sub>4</sub>.

Better knowledge of the current CH<sub>4</sub> budget helps to reduce uncertainties in future projections of climate change and tropospheric

ozone evolution and to design effective mitigation strategies. Atmospheric long-term measurements and inverse models currently provide key information for assessing CH<sub>4</sub> emission trends at the global to subcontinental scale. Given uncertainties in surface emissions and OH distribution, however, using this approach at the regional or country scale remains challenging and requires an observational network that is dense in space and time<sup>27</sup>. In the future, the combined use of improved emission inventories, isotopic observations and global space-borne measurements of column-integrated CH<sub>4</sub> should help better to quantify regional sources, to separate natural from anthropogenic processes, and to verify the effectiveness of CH<sub>4</sub> mitigation policies.

## METHODS

**Inversion model setup.** The inverse methodology has been fully described<sup>19</sup> through the example of OH field optimization against methyl chloroform observations. For CH<sub>4</sub>, surface emissions are optimized each month for 11 land regions (those defined in ref. 28), one global ocean region, and up to ten processes over each land region (emissions from bogs, swamps, tundra, termites, fossil fuel and industry, gas, bio-fuel, ruminant animals, landfills and waste, and soil uptake). This spatial partition enables us to perform both geographically based and process-based analyses. On a geographical basis, the optimized emissions were further aggregated, after inversion, over three large regions: northern regions (boreal & temperate North America, boreal & temperate Asia, and Europe, roughly >30°N), tropical regions (tropical America, north and South Africa, tropical Asia), and southern regions (temperate South America and Oceania, roughly <30°S). We used the optimized interannual four-dimensional distribution of OH from ref. 19. The variations in OH are pre-optimized from methyl chloroform data using interannual winds and chemistry (see Supplementary Information). In this procedure, the inferred interannual OH fields also depend on methyl chloroform sources. Uptake of CH<sub>4</sub> by soils is optimized as an independent sink, but we do not explicitly solve for the stratospheric sink of CH<sub>4</sub> but assume that it is included in the removal by the stratospheric OH radicals of the INCA model<sup>17</sup>.

Atmospheric CH<sub>4</sub> observations, from roughly weekly air samples collected in flasks, were inverted as monthly means. Uncertainties in the monthly means were taken from the GLOBALVIEW-CH<sub>4</sub> data product<sup>29</sup>, when available, or from submonthly variability in the measurements. In total, data from 68 sites from different networks were collected and used; 75% was contributed by the NOAA network. Offsets between different observing networks were accounted for by using intercomparison round-robin information reported in GLOBALVIEW-CH<sub>4</sub>. The sampling periods for each site, and data uncertainties, are given in Supplementary Table A2. Atmospheric δ<sup>13</sup>C-CH<sub>4</sub> flask data from 13 NOAA sites were used in the inversion for the 1998–2004 period (Supplementary Table A2). The δ<sup>13</sup>C-CH<sub>4</sub> values were measured by INSTAAR at the University of Colorado<sup>30</sup>. At four sites (Point Barrow, Mauna Loa, Samoa and South Pole), the NOAA observations were merged with those from the SIL network<sup>31</sup> to extend the time series for the period 1989–2004. The gap in δ<sup>13</sup>C-CH<sub>4</sub> data in the period with no observations in 1996–1997 was filled by interpolation, and the interpolated values associated with a large *a priori* uncertainty in the inversion. At Niwot Ridge, the UCI network time-series<sup>32</sup> was used to extend the atmospheric δ<sup>13</sup>C-CH<sub>4</sub> record back to 1994. Although isotopic ratios are monitored at only 13 sites, they are expected to constrain usefully the partitioning of CH<sub>4</sub> sources according to their mean isotopic signature: biomass burning (about –20‰ for C-3 plants; about –12‰ for C-4 plants), all bacterial processes (about –60‰) and fossil-fuel-related sources (about –40‰), the atmosphere being close to –47‰ on average. The carbon isotopes measurements are relative to Vienna Pee Dee Belemnite (VPDB).

The inversion of CH<sub>4</sub> fluxes accounts for the fact that CH<sub>4</sub> removal by OH radicals is a nonlinear function of surface CH<sub>4</sub> emissions, by iteratively applying the forward and the inverse transport chemistry model up until convergence is reached for the OH removal of CH<sub>4</sub>. In inversions using δ<sup>13</sup>C-CH<sub>4</sub> data, we account for the fact that transport and chemistry of δ<sup>13</sup>C-CH<sub>4</sub> is nonlinear by solving iteratively for both the underlying CH<sub>4</sub> source magnitude and its isotopic composition, as in ref. 33.

**Sensitivity tests.** The settings of the inversion model that were varied in the sensitivity tests were (1) the *a priori* error on regional fluxes; (2) the *a priori* error on the atmospheric CH<sub>4</sub> and δ<sup>13</sup>C-CH<sub>4</sub> measurements; (3) the number of land regions to be optimized; (4) the size of the atmospheric network; (5) the use of non interannual transport; (6) the uses of non-interannual OH; (7) the introduction of an additional source due to possible CH<sub>4</sub> emission by plants<sup>22</sup>. See Supplementary Table A2 for a complete description of the 18 inversions performed.

**NSD.** The normalized standard deviation (NSD) is calculated as the ratio between the s.d. of the monthly deseasonalized inverted CH<sub>4</sub> flux anomaly and the s.d. of the same anomaly calculated by the bottom-up model. An NSD value of 1 indicates a similar variability between the inversion and the bottom-up model.

Received 10 April; accepted 3 August 2006.

1. IPCC. *Climate Change 2001: The Scientific Basis. Contribution of Working Group I to the Third Assessment Report of the Intergovernmental Panel on Climate Change* (eds Houghton, J. T. et al.) (Cambridge Univ. Press, Cambridge and New York, 2001).
2. Dlugokencky, E. J. et al. Atmospheric methane levels off: temporary pause or a new steady-state? *Geophys. Res. Lett.* **30**, 1992, doi:10.1029/2003GL018126 (2003).
3. Dentener, F. et al. Interannual variability and trend of CH<sub>4</sub> lifetime as a measure for OH changes in the 1979–1993 time period. *J. Geophys. Res.* **108**, 4442, doi:10.1029/2002JD002916 (2003).
4. Dlugokencky, E. J. et al. Changes in CH<sub>4</sub> and CO growth rates after the eruption of Mt Pinatubo and their link with changes in tropical tropospheric UV flux. *Geophys. Res. Lett.* **23**, 2761–2764 (1996).
5. Dlugokencky, E. J. et al. A dramatic decrease in the growth-rate of atmospheric methane in the Northern-Hemisphere during 1992. *Geophys. Res. Lett.* **21**, 507–507 (1994).
6. Langenfelds, R. L. et al. Interannual growth rate variations of atmospheric CO<sub>2</sub> and its δ C-13, H-2, CH<sub>4</sub>, and CO between 1992 and 1999 linked to biomass burning. *Glob. Biogeochem. Cycles* **16**, 1048, doi:10.1029/2001GB001466 (2002).
7. Manning, M. R., Lowe, D. C., Moss, R. C., Bodeker, G. E. & Allan, W. Short-term variations in the oxidizing power of the atmosphere. *Nature* **436**, 1001–1004 (2005).
8. Page, S. E. et al. The amount of carbon released from peat and forest fires in Indonesia during 1997. *Nature* **420**, 61–65 (2002).
9. Van der Werf, G. R. et al. Continental-scale partitioning of fire emissions during the 1997 to 2001 El Niño/La Niña period. *Science* **303**, 73–76 (2004).
10. Walter, B. P., Heimann, M. & Matthews, E. Modeling modern methane emissions from natural wetlands 2. Interannual variations 1982–1993. *J. Geophys. Res.* **106**, 34207–34219 (2001).
11. Wang, J. S. et al. A 3-D model analysis of the slowdown and interannual variability in the methane growth rate from 1988 to 1997. *Glob. Biogeochem. Cycles* **18**, 3011, doi:10.1029/2003GB002180 (2004).
12. Warwick, N. J., Bekki, S., Law, K. S., Nisbet, E. G. & Pyle, J. A. The impact of meteorology on the interannual growth rate of atmospheric methane. *Geophys. Res. Lett.* **29**, 1947, doi:10.1029/2002GL015282 (2002).
13. Chen, Y. H. & Prinn, R. G. Estimation of atmospheric methane emissions between 1996 and 2001 using a three-dimensional global chemical transport model. *J. Geophys. Res.* **111**, doi:10.1029/2005JD006058 (2006).
14. Mikaloff Fletcher, S. E. M., Tans, P. P., Bruhwiler, L. M., Miller, J. B. & Heimann, M. CH<sub>4</sub> sources estimated from atmospheric observations of CH<sub>4</sub> and its C-13/C-12 isotopic ratios: 1. Inverse modeling of source processes. *Glob. Biogeochem. Cycles* **18**, GB4004, doi:10.1029/2004GB002223 (2004).
15. Simmonds, P. G. et al. A burning question. Can recent growth rate anomalies in the greenhouse gases be attributed to large-scale biomass burning events? *Atmos. Environ.* **39**, 2513–2517 (2005).
16. Butler, T. M., Rayner, P. J., Simmonds, I. & Lawrence, M. G. Simultaneous mass balance inverse modeling of methane and carbon monoxide. *J. Geophys. Res.* **110**, D21310, doi:10.1029/2005JD006071 (2005).
17. Hauglustaine, D. A. et al. Interactive chemistry in the Laboratoire de Meteorologie Dynamique general circulation model: description and background tropospheric chemistry evaluation. *J. Geophys. Res.* **109**, D04314, doi:10.1029/2003JD003957 (2004).
18. Uppala, S. M. et al. The ERA-40 reanalysis. *Q. J. R. Meteorol. Soc.* **131**, 2961–3012 (2005).
19. Bousquet, P., Hauglustaine, D. A., Peylin, P., Carouge, C. & Ciais, P. Two decades of OH variability as inferred by an inversion of atmospheric transport and chemistry of methyl chloroform. *Atmos. Chem. Phys.* **5**, 2635–2656 (2005).
20. Bousquet, P. et al. Regional changes in carbon dioxide fluxes of land and oceans since 1980. *Science* **290**, 1342–1346 (2000).
21. Rodenbeck, C., Houweling, S., Gloor, M. & Heimann, M. CO<sub>2</sub> flux history 1982–2001 inferred from atmospheric data using a global inversion of atmospheric transport. *Atmos. Chem. Phys.* **3**, 1919–1964 (2003).
22. Keppler, F., Hamilton, J. T. G., Braß, M. & Rockmann, T. Methane emissions from terrestrial plants under aerobic conditions. *Nature* **439**, 187–191 (2006).
23. Prigent, C., Matthews, E., Aires, F. & Rossow, W. B. Remote sensing of global wetland dynamics with multiple satellite data sets. *Geophys. Res. Lett.* **28**, 4631–4634, doi:10.1029/2001GL013263 (2001).
24. Hoerling, M. & Kumar, A. The perfect ocean for drought. *Science* **299**, 691–694 (2003).
25. Hansen, J., Ruedy, R., Sato, M. & Reynolds, R. Global surface air temperature in 1995: return to pre-Pinatubo level. *Geophys. Res. Lett.* **23**, 1665–1668 (1996).
26. Dlugokencky, E. J., Steele, L. P., Lang, P. M. & Masarie, K. A. The growth-rate and distribution of atmospheric methane. *J. Geophys. Res.* **99**, 17021–17043 (1994).

27. Bergamaschi, P. *et al.* Inverse modelling of national and European CH<sub>4</sub> emissions using the atmospheric zoom model TM5. *Atmos. Chem. Phys.* **5**, 2431–2460 (2005).
28. Gurney, K. R. *et al.* Towards robust regional estimates of CO<sub>2</sub> sources and sinks using atmospheric transport models. *Nature* **415**, 626–630 (2002).
29. GLOBALVIEW-CH<sub>4</sub>. *Cooperative Atmospheric Data Integration Project—Methane CD-ROM* (NOAA/CMDL, Boulder, CO, 2005).
30. Miller, J. B. *et al.* Development of analytical methods and measurements of C-13/C-12 in atmospheric CH<sub>4</sub> from the NOAA Climate Monitoring and Diagnostics Laboratory global air sampling network. *J. Geophys. Res.* **107**, 4178, doi:10.1029/2001JD000630 (2002).
31. Quay, P. *et al.* The isotopic composition of atmospheric methane. *Glob. Biogeochem. Cycles* **13**, 445–461 (1999).
32. Tyler, S. C. *et al.* Stable carbon isotopic composition of atmospheric methane: a comparison of surface level and free tropospheric air. *J. Geophys. Res.* **104**, 13895–13910 (1999).
33. Hein, R., Crutzen, P. J. & Heimann, M. An inverse modeling approach to investigate the global atmospheric methane cycle. *Glob. Biogeochem. Cycles* **11**, 43–76 (1997).

**Supplementary Information** is linked to the online version of the paper at [www.nature.com/nature](http://www.nature.com/nature).

**Acknowledgements** We thank P. Rayner, F. Chevallier and F.-M. Breon for comments on the manuscript, and P. Quay for published  $\delta^{13}\text{C}$ -CH<sub>4</sub>

measurements for the period 1989–1995. Atmospheric CH<sub>4</sub> measurements from Réseau Atmosphérique de Mesure des Composés à Effet de Serre (RAMCES) at Laboratoire des Sciences du Climat et de l'Environnement (LSCE) were partly funded by Institut National des Sciences de l'Univers (INSU). All calculations were realized with Commissariat à l'Energie Atomique (CEA), Centre National de la Recherche Scientifique (CNRS), Institut Pierre Simon Laplace (IPSL) and LSCE computers and support. The development of the Global Fire Emissions Dataset (GFED) used here was supported by a grant from the National Aeronautics and Space Administration (NASA).

**Author Contributions** The main contributions of each author are: P.B.: inversions, data analysis and coordination. P.C.: inverse method and manuscript improvements. J.B.M.: CH<sub>4</sub> and  $\delta^{13}\text{C}$ -CH<sub>4</sub> data analysis and inversion analysis. E.J.D.: CH<sub>4</sub> measurements and manuscript improvements. D.A.H.: chemistry-transport model and manuscript improvements. C.P. and F.P.: satellite retrievals of flooded areas. G.R.V.d.W.: CH<sub>4</sub> emissions from fires. P.P. and C.C.: inversion method. R.L.L.: CH<sub>4</sub> measurements and manuscript improvements. E.G.B., M.R., M.S., L.P.S. and S.C.T.: CH<sub>4</sub> measurements. J.L.: plant source analysis. J.W.:  $\delta^{13}\text{C}$ -CH<sub>4</sub> measurements.

**Author Information** Reprints and permissions information is available at [www.nature.com/reprints](http://www.nature.com/reprints). The authors declare no competing financial interests. Correspondence and requests for materials should be addressed to P.B. ([philippe.bousquet@cea.fr](mailto:philippe.bousquet@cea.fr)).

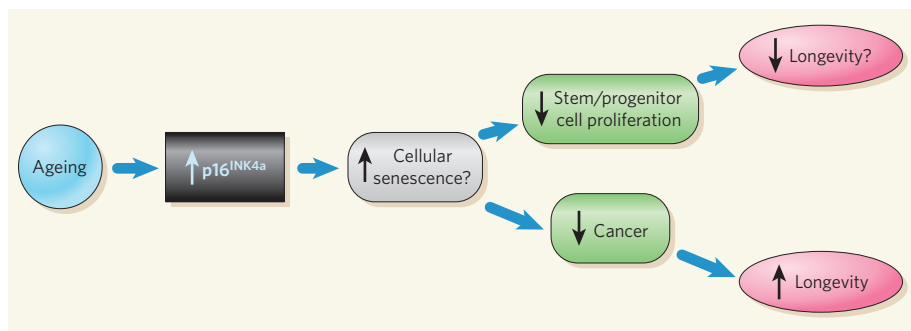


**Figure 1 | Dual activities of p16<sup>INK4a</sup> during ageing.** Ageing causes an increase in p16<sup>INK4a</sup>, a potent tumour suppressor that promotes longevity by suppressing the development of cancer. Three papers show that p16<sup>INK4a</sup> suppresses the proliferation of stem or progenitor cells in the bone marrow, pancreas and brain<sup>3–5</sup>. The mechanisms that induce p16<sup>INK4a</sup> during ageing are not known (black box). Once expressed, p16<sup>INK4a</sup> causes cellular senescence (grey box), a permanent growth-arrested state, which may be the mechanism by which this protein suppresses the proliferation of stem/progenitor cells. The decline in stem/progenitor-cell proliferation compromises tissue regeneration and repair, which is likely to reduce longevity.

the potential to form new SVZ neurons. However, p16<sup>INK4a</sup> deficiency did not prevent age-associated declines in cell proliferation in the dentate gyrus region of the brain or the enteric nerves in the gut, so different mechanisms may drive the ageing of stem/progenitor cells in other parts of the nervous system.

These three papers uncover a novel role for the p16<sup>INK4a</sup> tumour suppressor in promoting ageing (Fig. 1), a role shared by the p53 tumour suppressor<sup>9,10</sup>. But they also raise many questions. Does p16<sup>INK4a</sup> drive stem/progenitor-cell

ageing by inducing an irreversible senescence arrest, a reversible quiescent state or another mechanism? What causes the age-dependent rise in p16<sup>INK4a</sup> expression? Is it induced by hormones such as those that regulate the insulin/IGF pathway during ageing<sup>11</sup>? Or is it caused by stress or damage signals within the cells? Given that p16<sup>INK4a</sup> deficiency only partly mitigates most of the ageing effects studied, what other mechanisms cause stem/progenitor-cell ageing? Finally, how important is the ageing of cells, in this case stem/progenitor cells, for the longevity

of an organism? Does it depend on the type or level of stress that the organism experiences?

Answers to these questions might clarify whether drugs that blunt p16<sup>INK4a</sup> expression or activity will ameliorate certain age-related diseases. Whatever the answers, it is important to remember that p16<sup>INK4a</sup>-deficient mice frequently succumb to cancer in mid-life (1.5–2 years). We will therefore need to know much more about the regulators and effectors of p16<sup>INK4a</sup> before these remarkable findings can be harnessed to make effective longevity-promoting therapies.

Christian M. Beausejour is at the Centre de recherche pédiatrique, Hôpital Sainte-Justine, Université de Montréal, 3175 chemin de la Côte-Sainte-Catherine, Montréal H3T 1C5, Canada. Judith Campisi is at the Lawrence Berkeley National Laboratory, 1 Cyclotron Road, Berkeley, California 94720, USA, and the Buck Institute for Age Research. e-mail: jcampisi@lbl.gov

1. Krtolica, A. *Int. J. Biochem. Cell Biol.* **37**, 935–941 (2005).
2. Campisi, J. *Nature Rev. Cancer* **3**, 339–349 (2003).
3. Janzen, V. *et al. Nature* **443**, 421–426 (2006).
4. Krishnamurthy, J. *et al. Nature* **443**, 453–457 (2006).
5. Molofsky, A. V. *et al. Nature* **443**, 448–452 (2006).
6. Collins, C. J. & Sedivy, J. M. *Ageing Cell* **2**, 145–150 (2003).
7. Campisi, J. *Cell* **120**, 1–10 (2005).
8. Krishnamurthy, J. *et al.* **114**, 1299–1307 (2004).
9. Tyner, S. D. *et al. Nature* **415**, 45–53 (2002).
10. Maier, B. *et al. Genes Dev.* **18**, 306–319 (2004).
11. Bartke, A. *Endocrinology* **146**, 3718–3723 (2005).

## CLIMATE CHANGE

# A nasty surprise in the greenhouse

Jos Lelieveld

**The Kyoto Protocol aims to reduce emissions of greenhouse gases such as methane. But it seems that the fall in human-induced methane emissions in the 1990s was only transitory, and atmospheric methane might rise again.**

Methane is a potent greenhouse gas — per molecule, more than 20 times as powerful as carbon dioxide<sup>1</sup>. Moreover, when methane emissions rise, so too does the concentration of the pollutant ozone in the troposphere, the lowest layer of Earth's atmosphere<sup>2</sup>. Methane also consumes hydroxyl radicals, whose oxidative effects are essential to atmospheric cleansing. On page 439 of this issue<sup>3</sup>, Bousquet *et al.* recount the results of an international effort to measure atmospheric methane concentrations and combine these data with a computer model of atmospheric chemistry and transport. The bad news is that the slowdown in global methane emissions in the past few decades was only temporary: reports of the emissions' control have been exaggerated.

At present, about two-thirds of global methane comes from anthropogenic sources, and most emissions occur in the Northern Hemisphere (Fig. 1, overleaf). Of naturally produced

methane, the largest proportion stems from bacteria in wetlands that produce the gas when decomposing organic material. The growth rate of atmospheric methane was more than 10% per decade before 1980, but by the 1990s it had dropped to nearly zero (Fig. 2, overleaf)<sup>4</sup>. Bousquet and colleagues<sup>3</sup> compute the global methane source distribution, especially its variability over recent decades. This is a rather controversial issue, as it is difficult to determine whether this variability should be attributed to fluctuations in the sources or in the sinks; the sink mechanisms are dominated by the good offices of the atmospheric hydroxyl radicals<sup>5</sup>.

The authors used a so-called inversion modelling technique, which starts from observed concentrations at Earth's surface and back-calculates using models of transport and loss processes to optimize source estimates. The measurements stem from a global network

of monitoring stations, and include isotope data (in particular, the relative proportion of carbon-13) that provide an additional clue as to what methane came from where. Methane from biomass burning, fossil-fuel-related sources and bacterial processes have distinct isotopic signatures; methane emissions from wetlands, for example, are substantially depleted in carbon-13.

The approach is novel because the model computations optimized both methane emissions and methane loss through hydroxyl oxidation. The crux of the findings is that fluctuations of natural emissions, in particular by wetlands in the tropics, are a dominant factor in the variability of methane from year to year. These emissions are in turn sensitive to meteorological parameters: during dry periods, methane flux from wetlands is depressed.

Thus, during the most recent part of the analysis period — from 1999 onward — extended droughts have reduced natural methane emissions. This has concealed the fact that anthropogenic emissions have resumed their increase, an increase perhaps associated with the accelerating use of fossil fuels by booming Asian economies. Continued monitoring of atmospheric methane, and especially its relation to wetland inundation and drying, will be needed to substantiate this prediction.

Bousquet and colleagues' study<sup>3</sup> is not incompatible with the recent suggestion that

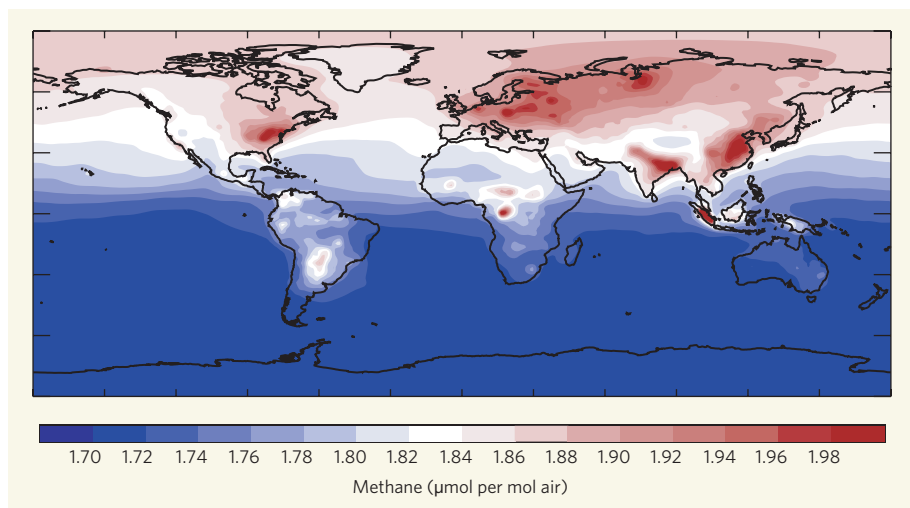


**Figure 1 | Methane hotspots.** Average methane mixing ratios in the boundary layer (the layer of the atmosphere in immediate contact with Earth's surface) in 2003, calculated with a chemistry–transport model. The atmospheric lifetime of methane is almost a decade, so it disperses globally. Regions of strong emissions are nevertheless manifest, leading to the largest variability in the Northern Hemisphere and an inter-hemispheric difference of 5–10%. The recently proposed release of methane by terrestrial vegetation is not included, as its magnitude is still uncertain. (Figure courtesy S. Houweling<sup>5</sup>.)

terrestrial vegetation is a strong methane source<sup>6</sup>. It sounds paradoxical that adding a large new source such as this, which contributes 30% of the global methane flux to the model, and decreasing the others proportionately can be done without fundamentally changing the inversion calculations. But the combination of the relatively strong meridional methane gradient (Fig. 2) and too few measurement stations in the tropics makes constraining the size of single-source categories such as forests and wetlands tricky.

Further confirmation of a large vegetation source comes from satellite measurements showing that methane concentrations are enhanced over the tropical rainforests<sup>7</sup>. It is remarkable not only that this large new methane source has just been discovered, but also that mechanisms for producing methane deviate from the known anaerobic formation by microbes. The role of oxygen in methanogenesis, including its application in renewable energy production, should receive much more attention in the coming years.

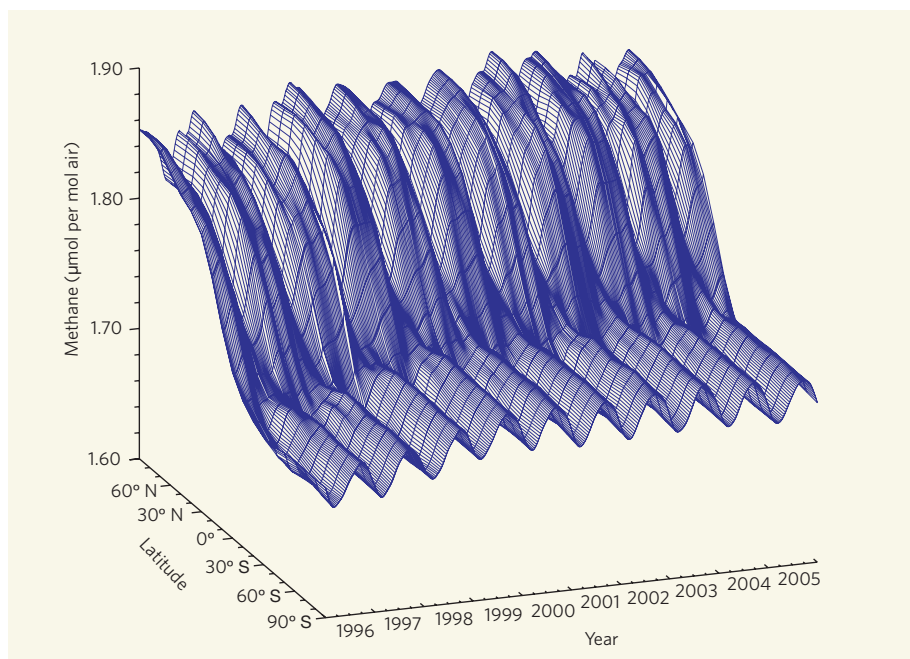


**Figure 2 | Meridional slide.** The latitudinal methane distribution in the marine boundary layer over the past 10 years, based on measurements in the air-sampling network of the Earth System Research Laboratory of the US National Oceanic and Atmospheric Administration. Annual fluctuations and the higher methane concentrations at higher northern latitudes are clear, but over the period surveyed, the year-on-year trend is small. Bousquet *et al.*<sup>3</sup> suggest that recent dry years have led to a drop in natural methane emissions, masking a rise in emissions induced by human activities. (Figure courtesy E. Dlugokencky<sup>4</sup>.)

Atmospheric methane is a factor in the amplification of climate change, because the amount of methane released by wetlands and vegetation responds sensitively to temperature and moisture conditions. This establishes a positive-feedback mechanism that has contributed to rapid climate shifts during the last glacial cycle<sup>8</sup>. But Bousquet and colleagues' analysis<sup>3</sup> also allows for a negative-feedback mechanism, put in place by atmospheric chemistry. In dry periods of reduced methane emissions, methane removal by hydroxyl radicals also decreases. The dryness aggravates vegetation fires, which release large amounts of carbon monoxide, and this pollutant gas also consumes hydroxyl. With less hydroxyl around, less methane is broken down, and the decrease in methane concentration is not as large as might be expected.

This phenomenon is not natural, however: most fires are ignited by humans. Furthermore, vast amounts of methane are deposited as hydrates in permafrost regions and in marine sediments. It is as yet unclear to what extent the melting of permafrost and increasing ocean temperature will affect these methane reservoirs, destabilize the hydrates and exacerbate greenhouse warming. These processes influence both atmospheric methane and hydroxyl, and are potentially important feedback mechanisms that require further research.

It will be both essential and difficult to control greenhouse-gas emissions and verify nationally reported inventories. Human-induced emissions scale with fossil-fuel consumption, and the global yearning for energy, especially in nations that do not recognize the Kyoto Protocol on climate change, gives rise to concern about climate change. The uncertainty range associated with climate projections<sup>1</sup> implies that large changes will be as likely as modest ones. Such large and possibly disruptive climate changes ask for short-term solutions.

Unfortunately, the response times of most greenhouse gases in the atmosphere and their climatic effects are slow — decades to centuries. Measures to control methane emissions should be placed high on the agenda because they, in contrast, become effective within a few years. In a situation where climate change is accelerating, there is no time to lose: we need effective solutions, and we must act fast. ■

Jos Lelieveld is at the Max-Planck-Institut für Chemie, Johann-Joachim-Becher-Weg 27, 55128 Mainz, Germany.  
e-mail: lelieveld@mpch-mainz.mpg.de

1. Ramaswamy, V. *et al.* in *Climate Change 2001: The Third Assessment Report of the Intergovernmental Panel on Climate Change* (eds Houghton, J. T. *et al.*) 349–416 (Cambridge Univ. Press, 2001).
2. Lelieveld, J., Crutzen, P. J. & Dentener, F. J. *Tellus* **50B**, 128–150 (1998).
3. Bousquet, P. *et al.* *Nature* **443**, 439–443 (2006).
4. Dlugokencky, E. J. *et al.* *Geophys. Res. Lett.* **30**, 1992 (2003).
5. Houweling, S. *et al.* *J. Geophys. Res.* **104**, 26137–26160 (1999).
6. Keppler, F. *et al.* *Nature* **439**, 187–191 (2006).
7. Frankenberg, C. *et al.* *Science* **308**, 1010–1014 (2005).
8. Brook, E. J. *et al.* *Glob. Biogeochem. Cycles* **14**, 559–572 (2000).

## SUPPLEMENTARY INFORMATION

### **Analysis of the observed CH<sub>4</sub> growth rate**

The observed CH<sub>4</sub> growth rate deduced from the NOAA global cooperative air sampling network<sup>1</sup> was averaged into three large latitude bands, (30-90°S, 30°S-30°N (Tropics), and 30-90°N), providing hints on the regions where changes occurred (Fig. 1a). For each latitude band, we calculated average trends in CH<sub>4</sub> differences between each NOAA site and South Pole (SPO). SPO was chosen as a reference because of its remoteness from sources. Before 1992, the CH<sub>4</sub> latitudinal differences were increasing with time both in the Tropics and northwards, with a large uncertainty due to the spread among sites (Fig. 1b). In contrast, after 1992, the CH<sub>4</sub> difference with SPO decreased in the Tropics, and decreased even more strongly north of 30°N, despite the 1997-1998 and 2002-2003 transient rises in CH<sub>4</sub> growth rates in the North (Fig 1a). This suggests that either northern emissions of methane declined persistently since 1992 or that its destruction by OH increased north of 30°N. More unlikely, enhanced inter-hemispheric mixing may also reduce North-South gradients of atmospheric gas, which is not observed for other long-lived greenhouse gases, but for CH<sub>4</sub>.

### **Ensemble of 18 inversions**

Inversion results depend on various settings. We constructed an ensemble of 18 inversions, each with different settings, to test the influence of inversion settings on the inverted CH<sub>4</sub> fluxes (Table A1). The spread of fluxes obtained through the different members of the ensemble is used to derive a measure of the uncertainty of the results. The different inversions of the ensemble are constructed as follows.

**I-01, control.** Surface fluxes are solved each month for 80 distinct sources and sinks (unknowns). The source space contains 11 geographic regions<sup>2</sup>. A given region contains several sources. There are, in total, 7 regions with fossil CH<sub>4</sub> emissions, 7 for gas, 5 for

biofuel use, 7 for ruminant animals, 7 for biomass burning, 7 for landfills and waste, 7 for tropical swamps, 7 for termites, 6 for rice paddies, 4 for arctic bogs, 4 for tundra, 7 for soil uptake, and 1 single ocean region.

OH sink is treated as 4 tri-dimensional zonal regions (North of 30°N, 0-30°N, 0-30°S, south of 30°S). OH variability is optimized against methyl-chloroform (MCF) observations in a preliminary inversion described in ref. 3. This work showed a large sensitivity of the optimized OH fields to prior uncertainties of methyl-chloroform emissions, as compared to prior uncertainties of OH radicals. Prescribing methyl-chloroform emissions with a very tight prior error produces large inter-annual variations in OH, as in previous studies<sup>4</sup>. Such large OH fluctuations were questioned by recent work in refs. 5, 6. Therefore, for the CH<sub>4</sub> inversion, we prescribed optimized OH fields calculated by letting both methyl-chloroform emissions and OH vary significantly (scenario I-15% of ref. 3 illustrated in their fig. 12a). This methyl-chloroform inversion produces 65% less OH variability than in ref. 4, in which MCF emissions are prescribed. We also tested the impact on the CH<sub>4</sub> inversion of holding OH fields constant from one year to the next (see I-02 below).

We do not directly optimize the stratospheric loss in this work but we assume that this sink is included in the term of destruction of CH<sub>4</sub> by stratospheric OH, as modelled in the INCA model up to 35 km height<sup>7</sup>.

The partition of sources and sinks allows us to diagnose per region and per process changes in the CH<sub>4</sub> budget. Inverting for several source processes regionally limits the aggregation error<sup>8</sup>. Aggregation error is crucial for CO<sub>2</sub> inversions where each point of the globe (except ice and desert) has a non zero probability to absorb or emit this gas, and could be decreased by solving for fluxes on a very large number of regions<sup>8</sup> with some a priori correlations between them. Aggregation error for CH<sub>4</sub> is less crucial because there is rather accurate a priori information on the locations of emitting grid points, at least for some sources (wetlands,

gas fields, rice paddies) within each large region. Further, many a priori CH<sub>4</sub> emission maps (animals, landfills, fires) are constructed using the same emission factors over a large region. This implies a prior correlation close to 1 between distant grid points within that region, and justifies the optimization of fluxes over large regions in the inversion.

No a priori inter-annual variability is assigned to regional fluxes, except for animal emissions. The total CH<sub>4</sub> emission by animals is constrained within loose errors to the annual estimates of the EDGAR3.0 data base<sup>9</sup> for the 1984-1995 period, and of the FAO database<sup>10</sup> for the 1996-2003 period. The a priori error on each monthly source is set to  $\pm 100\%$ . We placed however a (soft) constraint on the temporal evolution of anthropogenic emissions (fossil, landfills), ocean and termites by forcing month-to month differences of these sources not to exceed  $\pm 10\%$  of their a priori values<sup>11</sup>. This soft constraint acts as a low pass filter preventing emissions from varying unrealistically from one month to the next. However, it does not prevent regional emissions from being adjusted to match the atmospheric data. For rice paddies the constraint on monthly differences is relaxed to  $\pm 50\%$ . For wetlands and wildfires, the constraint is relaxed  $\pm 150\%$ . Atmospheric CH<sub>4</sub> data are from 68 sites distributed globally (Figure A1). The sites are from diverse networks. Atmospheric data get assimilated as the sites appear in the network. Monthly mean CH<sub>4</sub> at each site is used in the inversion, with errors prescribed from the GLOBALVIEW-CH<sub>4</sub> database<sup>12</sup>. For sites that are not part of this database, uncertainties are calculated from the standard deviation of the data used to calculate the monthly means. The uncertainties are modulated up to  $\pm 30\%$  depending on the number of samples per month when calculating the monthly mean. The uncertainties on the monthly averages are assumed to be uncorrelated

**I-02.** Same as I-01 but with no inter-annual variability of OH sink.

**I-03.** Only the longest records from the NOAA network are used compared to I-01 (50 sites listed in table A2 with more than 10 years of measurements; solid circles in Fig. A2).

Retaining only long records minimizes biases in inversion results caused by changes in the global network<sup>13</sup>.

**I-04.** 12 additional marine boundary layer measurement records (Table A2) are used to supplement the 50 NOAA sites used in I-03 (triangles in Fig. A2).

**I-05.** Same as I-04 but 4 additional continental sites with time series of only a few years (generally beginning the early 2000s) are added (squares in Fig. A2).

**I-06.** Same as I-01 but additional  $\delta^{13}\text{C-CH}_4$  observations at 13 sites are used (blue dots in fig. A1). Between 1998 and 2003, data are from the NOAA sites<sup>14</sup>. A mean monthly error of  $\pm 0.1\text{‰}$  and  $\pm 0.2\text{‰}$  is applied to  $\delta^{13}\text{C-CH}_4$  data in the southern hemisphere and in the northern hemisphere, respectively. These errors are increased when the number of flasks sampled each month decreases (Table A2). At three sites (BRW, CGO, MLO),  $\delta^{13}\text{C-CH}_4$  observations from the SIL network<sup>15</sup> over the 1988-1996 period are used to extend the NOAA-INSTAAR records. Despite the two year data gap in  $\delta^{13}\text{C-CH}_4$  in 1996-1997, we found no significant discontinuity between the NOAA and SIL records, and applied no bias correction to the data. The  $\delta^{13}\text{C-CH}_4$  flask data are filtered in the time domain<sup>16</sup> to retain only quasi-monthly changes, and fill in the 1996-1997 data gap (but errors are set to be very loose during the 1996-1997 gap as visible in Fig. A2). At NWR,  $\delta^{13}\text{C-CH}_4$  from the UCI network over 1995-2001<sup>17</sup> is used to extend the NOAA-INSTAAR records. The a priori isotopic signature of each source and sink of  $\text{CH}_4$  is set according to ref. 18, and a small error of  $\pm 2\text{‰}$  on each source type is chosen. The kinetic isotopic fractionation associated to removal of  $\text{CH}_4$  by OH is taken as in recent ref. 18 at  $5.4\text{‰}$ .

**I-07.** Same as I-06, but the kinetic isotopic fractionation associated to removal of  $\text{CH}_4$  by OH is decreased to  $4.9\text{‰}$ .

**I-08.** Same as I-06, but the Kinetic isotopic fractionation associated to removal of  $\text{CH}_4$  by OH is increased to  $5.9\text{‰}$ .

**I-09.** Same as I-01 but the *a priori* soft constraint on the month-to-month differences is not used for the *a priori* fluxes.

**I-10.** Same as I-01 but the *a priori* source error on each region is set 50% smaller.

**I-11.** Same as I-01 but the *a priori* source error on each region is set 50% higher.

**I-12.** Same as I-01 but the *a priori* observation error at each site is set 50% smaller.

**I-13.** Same as I-01 but the *a priori* observation error at each site is set 50% higher.

**I-14.** The *a priori* fluxes are grouped per source type only (17 unknowns per month).

**I-15.** The *a priori* fluxes are grouped per region only with a separation between anthropic and natural emissions (28 unknowns per month).

**I-16.** The *a priori* fluxes are grouped per source type over 3 geographic regions only: a high northern region sum of Boreal North America, Temperate North America, Boreal Eurasia, Temperate Eurasia, and Europe; a tropical region sum of Tropical South America, Tropical Africa, and Tropical Asia; a southern region sum of Temperate south America, Southern Africa, and Australia (34 unknowns per month)

**I-17.** Same as I-01 but with no inter-annual transport. Transport from 1998 is recycled over time to calculate source response function. 1998 was chosen as the year giving the largest differences in inferred sources compared to inversion I-01 (among all years after 1990).

**I-18.** Same as I-01 but using an additional CH<sub>4</sub> source from plants (see text below).

### **Global methane budget and long term mean fluxes**

We estimated global methane emissions of  $525 \pm 8 \pm 6$  TgCH<sub>4</sub>/yr over the 1984-2003 period, with a 485 TgCH<sub>4</sub>/yr sink due to OH radicals (Table A3). The first error estimates the mean of the error calculated by the inversion model; the second error estimate is the spread of the monthly fluxes from the 18 inversions. This estimate lies in the range of recently reported values of 500 to 600 TgCH<sub>4</sub>/yr<sup>19, 20</sup>. In each region, the spread of the 18 members of the

ensemble is generally smaller than the mean error calculated by the inversion (Table A3). This indicates that our results are robust to the various settings tested above. Two noticeable exceptions are observed for tropical South America and non tropical southern regions, which remain very sensitive to the inversion settings (Table A3). Emissions for northern regions (Boreal and temperate regions of the inversion model), Tropics (tropical regions of the inversion model), and southern regions (austral regions of the inversion model) are respectively of  $257 \pm 8 \pm 6$  TgCH<sub>4</sub>/yr,  $195 \pm 11 \pm 15$  TgCH<sub>4</sub>/yr and  $53 \pm 7 \pm 14$  TgCH<sub>4</sub>/yr. The northern total emissions are larger than the tropical ones, in agreement with ref. 21. The inversion increases energy related emissions ( $110 \pm 13 \pm 7$  TgCH<sub>4</sub>/yr), biomass burning ( $38 \pm 7 \pm 2$  TgCH<sub>4</sub>/yr) and decreases rice paddy emissions ( $31 \pm 5 \pm 2$  TgCH<sub>4</sub>/yr) compared to a priori estimates. The global natural wetland emissions remain stable ( $147 \pm 15 \pm 9$  TgCH<sub>4</sub>/yr), with an increase in tropical swamps ( $104 \pm 12 \pm 9$  TgCH<sub>4</sub>/yr) and a decrease of boreal bogs and tundra emissions ( $43 \pm 8 \pm 3$  TgCH<sub>4</sub>/yr). Analysis of long-term trend in emissions reveals a global positive trend in the 1980s ( $+1.3 \pm 0.3$  TgCH<sub>4</sub>/yr<sup>2</sup>) and a negative trend after 1992 ( $-1.0 \pm 0.2$  TgCH<sub>4</sub>/yr<sup>2</sup>). These trends are largely controlled by tropical and Eurasian regions, and by energy-related and wetland emissions (Table A2).

The error reduction (ratio of inversion errors to a priori errors) provides information on the constraint placed by atmospheric observations on each flux. We found a larger error reduction when aggregating optimized fluxes on a geographical basis compared to process-based aggregation. This is because geographical partition relies directly on atmospheric observed gradients whereas process partition relies on the differences in the spatial patterns of emissions (sometimes over the same region) and on few isotopic measurements. We also found 1) an important error reduction (~50%) for wetlands and for non tropical regions, 2) a significant error reduction (~30%) for biomass burning and for tropical regions, and 3) a small

error reduction for most individual processes (rice cultivation, animals, termites, biofuel use, energy and landfills).

Analysis of a posteriori error covariance on the fluxes provides more hints. At the spatial aggregation level of the inversion (80 sources are solved), small negative error correlations are found between processes within a region, or between regions for the same process (e.g., North Asian bogs and European bogs,  $r=-0.46$ ; North Asia landfills vs. North Asia fossils  $r=-0.38$ ). This indicates qualitatively that the inversion may have difficulty to fully separate these regions/processes and may only constrain their sum. However, all annual error correlations remain small, below 0.5 in absolute values.

Finally, the use of  $\delta^{13}\text{C-CH}_4$  observations had two main effects on our inversion results: 1) the global biomass burning source increases significantly (+27%) compared to inversions without isotopes, and 2) the isotopic signature of the mean tropical source is reduced (-50.4‰ compared to -51.8‰ a priori) because of a decrease of the biomass burning emissions  $\delta^{13}\text{C}$  to -18.5‰, in the range of previous estimates, given the contribution of C4 plants in the Tropics<sup>18</sup>. In other regions, the inversion only slightly modifies the  $\delta^{13}\text{C}$  isotopic signatures. This may reflect the small prior error prescribed to the sources isotopic signature ( $\pm 2\%$ ) and the weak constraint placed by the available  $\delta^{13}\text{C-CH}_4$  observations on these signatures, as shown by the marginal error reductions on these terms.

### **Model for biomass burning flux over 1989-1995 based on CO atmospheric growth rates**

We compared inversion results with fire emissions estimated<sup>22</sup> from remotely-sensed fire counts and burned areas for the period 1996-2003, using the CASA ecosystem model<sup>23</sup>. Over the period 1989-1995, when no consistent global fire or  $\text{CH}_4$  emission product is available, we

used CO observations from the NOAA network, boldly assuming that all of the variability in atmospheric CO measurements is due to biomass burning<sup>24</sup>. Doing so, we calculated a scaling factor between the variability of observed CO growth rates, calculated as in ref. 16, and the one of known fire emissions<sup>23</sup> over 1996-2003. We then applied this factor to the observed CO trend before 1996 to extrapolate the variability of global CO emissions from fires since 1989. The variability in CH<sub>4</sub> emissions is then reconstructed using the CO:CH<sub>4</sub> mean emission ratio for 1996-2003.

### **Model for wetlands emissions of CH<sub>4</sub>**

A simple bottom-up wetland emission model was used to calculate inter-annual variations of CH<sub>4</sub> emissions by that source. Both the emission rates and the wetland spatial distribution (and their evolution in time) need to be estimated. For wetland distribution, we used monthly remote sensed estimates of flooded areas at 1° resolution based on observations of a suite of satellite observations, including passive and active microwave along with visible and infrared measurements<sup>25</sup>. A clustering technique that merges satellite observations is used to detect inundation. Monthly flooded areas, including natural wetlands and rice paddies, were then calculated by estimating pixel fractional coverage of flooding using the passive microwave signal and a linear mixture model with end-members calibrated with radar observations to account for vegetation cover. This satellite product is still under improvements by comparison with altimeter observations, surface temperature data, and precipitations. The period covered by this estimate is 1993-2001. For emission rates and emission seasons, we used the model described in ref. 26. For each partly flooded area 1° grid point, we determine the emission season and the CH<sub>4</sub> emission rate. For locations with zero freezing days during the year, mainly within the tropics, the emission season occurs when precipitation exceeds potential evaporation calculated from ref. 27. For locations with freezing days, the emission season

starts when surface air temperature exceeds 5°C. Emissions rates during the emission season were taken according to ref. 26 formulation :

$$k(T) = k(T_0) Q_{10}^{(T-T_0)/10}$$

where  $Q_{10}=2$ , and  $T_0=10^\circ\text{C}$ . Monthly input temperature and precipitation fields were taken from ECMWF ERA40 reanalysis at  $1.125^\circ$  <sup>28</sup>. We prescribed  $k(T_0)$  separately for bogs (mostly north of  $40^\circ\text{N}$ ) and for swamps wetlands (mostly south of  $40^\circ\text{N}$ ), according to scenario S3 of ref. 26, with a total of 35 TgCH<sub>4</sub>/yr for bog emissions and of 75 TgCH<sub>4</sub>/yr for swamps emissions. This gives  $k(T_0)=70$  mgCH<sub>4</sub>/m<sup>2</sup>/day for bogs and  $k(T_0)=240$  mgCH<sub>4</sub>/m<sup>2</sup>/day for swamps. These values of  $k(T_0)$  are larger than those used in ref. 26 because the flooded surfaces derived from satellite measurements appeared to be smaller than those used in ref. 26. Since flooded areas in ref. 25 comprise both natural and anthropogenic wetlands, we compared the bottom-up modeled estimate to the sum of inversion fluxes over wetlands and rice paddies. However, we did not directly account for rice paddy emission factors in the estimation of emission rates. This does not make a large difference because the interannual variability of rice paddies inferred by inversions is small compared to natural wetland variability. The bottom-up model provides monthly wetland CH<sub>4</sub> fluxes for the 1993-2001 period, the limitation being the availability of remotely sensed flooded areas. Overall, the variability of the bottom-up model is driven both by changes in flooded areas (~60%) and in emission rates (~40%).

### **Source of methane from plants**

A recent study suggested that CH<sub>4</sub> can be produced by plants under aerobic conditions<sup>29</sup>. We scaled up their emission factors for each type of vegetation, using the ORCHIDEE global

Global Vegetation Model<sup>30</sup>. The patterns of CH<sub>4</sub> emissions by plants follow the monthly Leaf Area Index values of ORCHIDEE, and the global value is set to +150 Tg CH<sub>4</sub>/yr<sup>29</sup>. We tested the impact of adding this vegetation source to the inversion (I-18, see table A2). The corresponding test inversion reduces the magnitude of the vegetation source by roughly 50 Tg/yr (compared to the a priori) while various other sources also get reduced by a total amount of 50 Tg/yr, so as to conserve the global emission (Table A3). The reduction of the plant source is especially sensitive over South America and South east Asia, whereas temperate and boreal emissions stay closer to the prior estimates. This indicates that the information contained in the current atmospheric network is not able to accurately separate long term-mean fluxes between different processes, even globally. However, we found that the latitudinal source distribution (NR, Tropics and SR) is more robustly constrained than the process-based distribution (Table A3).

Adding a new vegetation source has a different impact on the inverted variability, the main scope of the paper. The optimized global variability of vegetation emissions is  $\pm 10$  TgCH<sub>4</sub>/yr (Fig. A3). During the 1990s, inserting the plant source has only a marginal influence on the retrieval of wetlands and biomass burning flux anomalies (Fig. A3). The conclusions we draw on wetland and fires are thus affected little by the presence of a (uncertain) plant source. During the 1980's however, a new vegetation source would change the inferred wetland and fire anomalies, in presence of fewer sampling sites to separate the contribution of different processes (Fig. A3). This result also raises a caution flag on the large OH sink variations inferred from methyl-chloroform during the 1980s<sup>3, 6, 31</sup>. Over the whole 1984-2003 period, the variability in fossil fuel emissions (oil, gas, industry, coal, and bio-fuel) gets largely smoothed, but decadal changes remain robust when adding the plant source (Fig. A3). In short, adding a vegetation source increases the number of degrees of freedom available to

match the atmospheric variations: (1) some temporal variance is ‘transferred’ from the fossil to the vegetation source processes, (2) the inter-annual variability of wetlands and biomass burning emissions (at least for the 1990s) is marginally modified. A possible explanation is that both fossil fuel and plant CH<sub>4</sub> emissions are spatially more diffuse in space than fires or wetland emissions, and therefore more difficult to identify separately with the present-day atmospheric surface network.

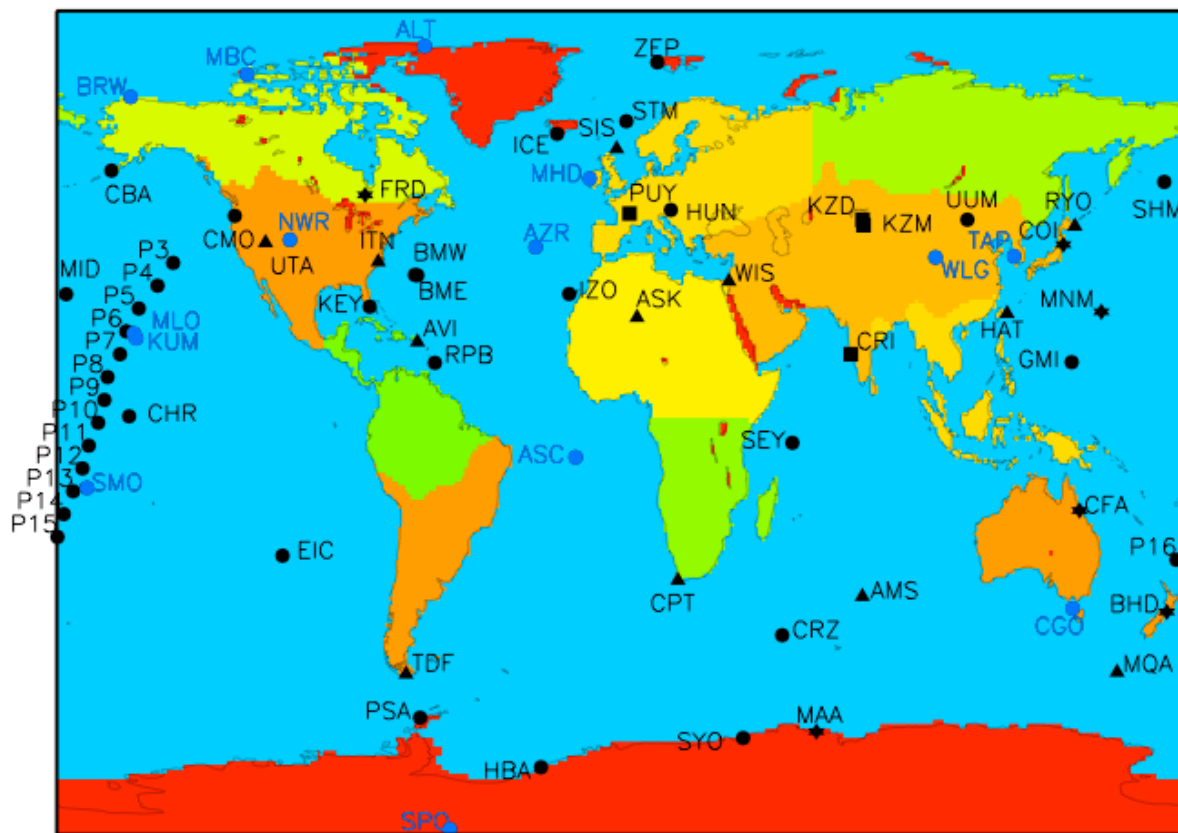


Figure A1: Map of the regions and the air sampling sites used in the 18 inversions. Different sets of sites were used in the inversion: 50 NOAA sites (black dots), 12 additional sites from other laboratories and/or shorter time series (triangles), 6 additional sites from other laboratories and/or shorter time series (stars) and 4 additional continental sites with short time series (squares). Sites with  $^{13}\text{C}$  measurements are plotted in blue. The 11 continental regions used to partition the  $\text{CH}_4$  correspond to those of the TRANSCOM3 model inter-comparison experiment<sup>2</sup>. One global ocean region was used, the ocean being a small net source of  $\text{CH}_4$ . Zero emissions are prescribed over Antarctica, Greenland and inner-seas and lakes (red color).

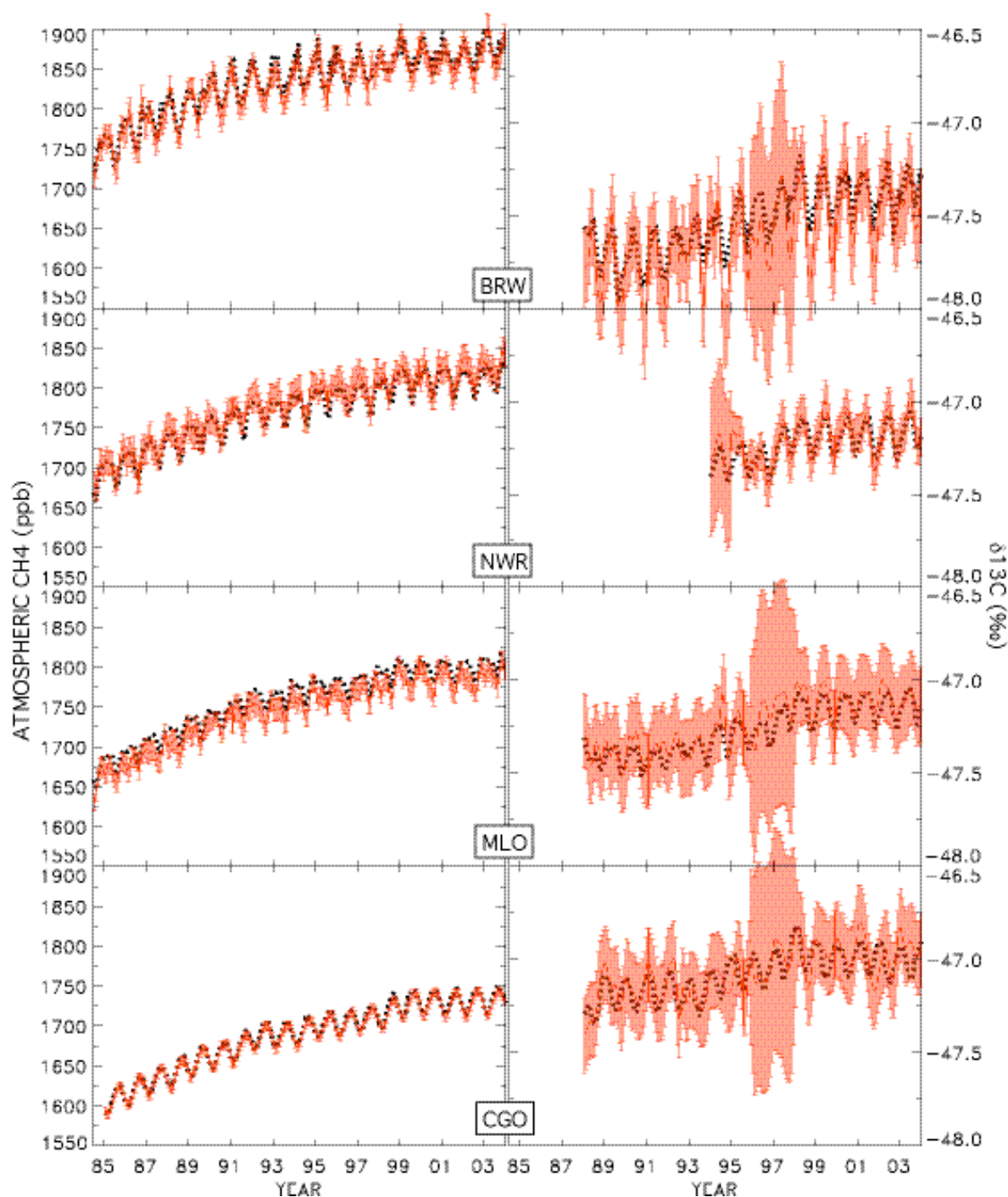


Figure A2: Fit of the inverse model to the observations. Optimized model (black) vs. observations (red) comparison at 4 sites for CH<sub>4</sub> (left) and <sup>13</sup>CH<sub>4</sub> (right): Barrow (BRW), Niwot Ridge (NWR), Mauna Loa (MLO) and Cape Grim (CGO). Error bars represent monthly observation errors as prescribed in the inversion model. For <sup>13</sup>CH<sub>4</sub> measurements at BRW, MLO and CGO, periods with interpolated values are associated with very large uncertainties (1996-1997). Uncertainties are one standard deviation.

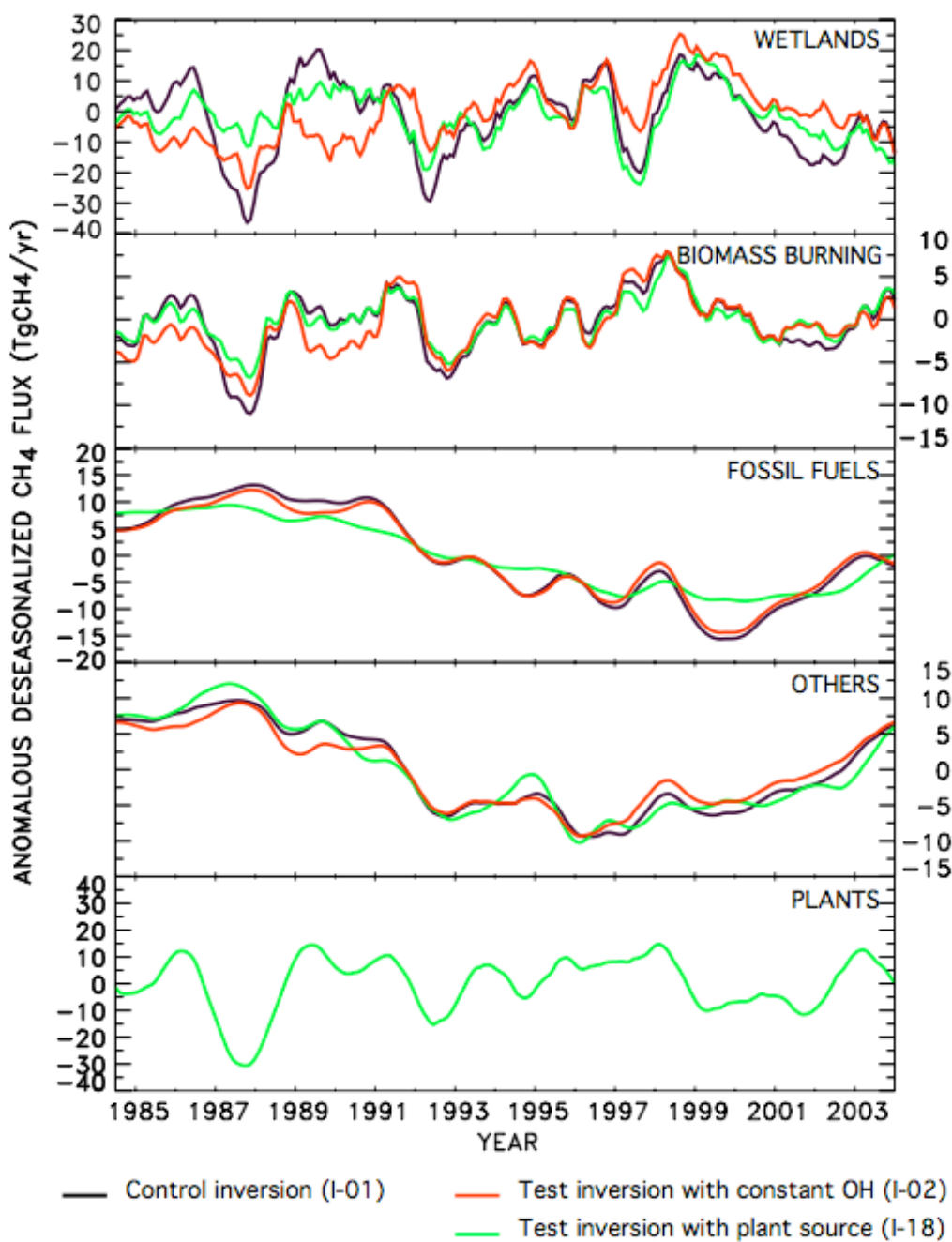


Figure A3: Sensitivity of inferred emissions to OH radicals and to possible additional emissions due to plants<sup>29</sup>. Inter-annual global CH<sub>4</sub> emission anomalies broken down (in TgCH<sub>4</sub>/yr) by process for three inversion scenarios: the control inversion (black), the test inversion with constant OH (red) and the test inversion using the plant source (green). The Y-axis are different in to clearly show the differences among the inversions.

INV I-XX	OBS	PROC/REGIONS	OBS ERROR	FLUX ERROR	OH IAV	TRANSPORT IAV
01	68	80	REF	REF	YES	YES
02	68	80	REF	REF	NO	YES
03	50 (NOAA)	80	REF	REF	YES	YES
04	62	80	REF	REF	YES	YES
05	72	80	REF	REF	YES	YES
06	68 + 13 ( <sup>13</sup> CH <sub>4</sub> )	80	REF	REF	YES	YES
07	68 + 13 ( <sup>13</sup> CH <sub>4</sub> )	80	REF	REF + low OH discrim	YES	YES
08	68 + 13 ( <sup>13</sup> CH <sub>4</sub> )	80	REF	REF + low OH discrim	YES	YES
09	68	80	No MMD	REF	YES	YES
10	68	80	REF	0.5*REF	YES	YES
11	68	80	REF	1.5*REF	YES	YES
12	68	80	0.5*REF	REF	YES	YES
13	68	80	1.5*REF	REF	YES	YES
14	68	17	REF	REF	YES	YES
15	68	28	REF	REF	YES	YES
16	68	34	REF	REF	YES	YES
17	68	80	REF	REF	YES	NO
18	68	87 Plant source added	REF	REF	YES	YES

Table A1: Main characteristics of the 18 inversions performed. « OBS » indicates the number of sites. « PROC/REGIONS » stand for the number of unknowns (process and/or regions) solved in the inversion. « OBS ERROR » and « FLUX ERROR » indicates the type of error used. If « OH IAV » is YES, OH varies from one year to the next according to the MCF optimisation described in ref. 3.

NAME	NETWORK	START	END	ERROR	NAME	NETWORK	START	END	ERROR
<b>I-03 : 50 sites</b>					<b>added in I-04 : 62 sites</b>				
alt	NOAA	1986	2004	9.0	ams	LSCE	1998	2003	3.1
asc	NOAA	1984	2004	5.4	ask	NOAA	1996	2003	8.2
azr	NOAA	1984	2004	13.0	avi	NOAA	1984	1989	13.7
bme	NOAA	1989	2003	18.5	coi	NIES	1996	2002	16.0
bmw	NOAA	1990	2003	16.2	cpt	SAWB-IFU	1984	2003	3.0
brw	NOAA	1984	2004	13.0	hat	NIES	1996	2004	22.1
cba	NOAA	1984	2003	10.0	itn	NOAA	1993	1998	30.8
cgo	NOAA	1985	2004	2.3	mqa	CSIRO	1991	2004	3.0
chr	NOAA	1985	2003	8.0	sis	CSIRO	1993	2003	8.0
cmo	NOAA	1984	1997	12.1	tdf	NOAA	1995	2002	3.0
crz	NOAA	1992	2003	1.7	uta	NOAA	1994	2003	25.2
eic	NOAA	1994	2002	2.3	wis	NOAA	1996	2003	26.9
gmi	NOAA	1984	2003	13.0	<b>added in I-01 (and other inversions) : 68 sites</b>				
hba	NOAA	1983	2002	1.4	bhd	NIWA	1990	2003	3.3
hun	NOAA	1994	2003	51.0	cfa	CSIRO	1992	2004	4.2
ice	NOAA	1993	2003	11.6	frd	AES	1990	2004	5.0
izo	NOAA	1992	2003	15.3	maa	CSIRO	1985	2004	4.9
key	NOAA	1984	2003	16.2	mnm	JMA	1994	2004	15.3
kum	NOAA	1984	2004	12.5	ryo	JMA	1996	2004	15.0
mbc	NOAA	1984	1996	9.0	<b>added in I-16 : 73 sites</b>				
mhd	NOAA	1992	2004	11.9	cri	CSIRO	1993	2001	5.4
mid	NOAA	1986	2003	14.2	kzd	NOAA	1998	2003	16.6
mlo	NOAA	1984	2004	11.2	kzm	NOAA	1998	2003	19.9
nwr	NOAA	1984	2004	16.1	puy	LSCE	2002	2004	15.0
poc000	NOAA	1987	2003	9.1	sch	IUP-UHEI	1997	2004	14.1
pocn05	NOAA	1987	2003	11.0	<b><sup>13</sup>CH<sub>4</sub> observations (I-05, I-06, I-07)</b>				
pocn10	NOAA	1987	2003	14.3	alt	NOAA	2001	2004	0.12
pocn15	NOAA	1987	2003	13.6	asc	NOAA	2001	2004	0.12
pocn20	NOAA	1987	2003	11.1	azr	NOAA	2001	2004	0.18
pocn25	NOAA	1987	2003	10.1	brw	NOAA/SIL	1988*	2004	0.25
pocn30	NOAA	1987	2003	12.7	cgo	NOAA/SIL	1988*	2004	0.25
pocs05	NOAA	1987	2003	7.6	kum	NOAA	1999	2004	0.15
pocs10	NOAA	1987	2003	7.6	mhd	NOAA	1999	2004	0.15
pocs15	NOAA	1987	2003	5.2	mlo	NOAA/SIL	1988*	2004	0.25
pocs20	NOAA	1987	2003	5.9	nwr	NOAA/UCI	1994*	2004	0.13
pocs25	NOAA	1987	2003	3.7	smo	NOAA	1998	2004	0.25
pocs30	NOAA	1987	2003	3.0	spo	NOAA	1998	2004	0.11
pocs35	NOAA	1987	2002	3.8	tap	NOAA	2001	2004	0.29
psa	NOAA	1983	2003	2.0	wlg	NOAA	2002	2004	0.13
rpb	NOAA	1988	2003	9.5					
sey	NOAA	1984	2003	11.5					
shm	NOAA	1986	2003	10.9					
smo	NOAA	1984	2004	7.5					
spo	NOAA	1983	2004	2.0					
stm	NOAA	1984	2003	12.3					
syo	NOAA	1987	2002	1.2					
tap	NOAA	1991	2004	29.4					
uum	NOAA	1992	2003	11.9					
wlg	NOAA	1992	2004	18.3					
zep	NOAA	1994	2003	9.2					
NAME	NETWORK	START	END	ERROR	NAME	NETWORK	START	END	ERROR

Table A2: Measurement sites used in the 18 inversions. "ERROR" is the mean monthly uncertainty (one standard deviation) used for each site. \*: <sup>13</sup>CH<sub>4</sub> sites for which NOAA records have been extended with other records (see text).

Period Unit	Long-term mean fluxes		Spread between ensemble members	Decadal average rate of change in fluxes		Source $\delta^{13}\text{C}$ signature		Test inv. with plant source
	1984-2003			1984-1991	1993-2003	1989-2003		
	<i>A priori</i>	<i>A posteriori</i>	TgCH <sub>4</sub> /yr	TgCH <sub>4</sub> /yr <sup>2</sup>		‰		TgCH <sub>4</sub> /yr
<b>Total source</b>	<b>497 ± 50</b>	<b>525 ± 8</b>	<b>6</b>	<b>+1.3 ± 0.3</b>	<b>-1.0 ± 0.2</b>	<b>-52.8</b>	<b>-51.5</b>	<b>535</b>
<b>Processes breakdown</b>								
Total wetlands	150 ± 30	147 ± 15	9	+1.1 ± 0.5	-0.6 ± 0.6	-58.0	-58.0	103
Swamps	90 ± 20	104 ± 12	9	-0.1 ± 0.5	-0.6 ± 0.4	-58.0	-57.9	80
Bogs and Tundra	60 ± 20	43 ± 8	3	+1.1 ± 0.4	-0.1 ± 0.4	-58.0	-58.1	22
Rice agriculture	39 ± 6	31 ± 5	2	-1.0 ± 0.3	-0.6 ± 0.4	-63.0	-62.8	31
Ruminant animals	90 ± 15	90 ± 14	2	+0.6 ± 0.2	+0.1 ± 0.3	-60.0	-59.9	88
Termites	20 ± 4	23 ± 4	2	+0.1 ± 0.1	+0.1 ± 0.1	-70.0	-69.9	20
Biomass burning	28 ± 10	38 ± 7	2	+0.5 ± 0.5	-0.1 ± 0.1	-19.0	-18.5	27
Bio-fuels	12 ± 4	12 ± 4	2	+0.0 ± 0.3	+0.0 ± 0.3	-37.0	-36.9	11
Energy	91 ± 14	110 ± 13	7	+0.9 ± 0.5	-0.8 ± 1.0	-40.4	-40.6	87
Coal & industry	47 ± 10	47 ± 10	5	+0.0 ± 0.2	-1.2 ± 1.0	-37.0	-36.9	41
Natural gas	44 ± 10	63 ± 9	5	+0.8 ± 0.3	+0.4 ± 0.4	-44.0	-43.9	46
Landfills & waste	50 ± 11	55 ± 11	5	-1.0 ± 0.6	+0.8 ± 1.0	-55.0	-54.8	46
Ocean	15 ± 6	19 ± 6	2	+0.0 ± 0.3	+0.0 ± 0.3	-60.0	-60.0	18
Plants								104
<b>Geographic breakdown</b>								
NR	264 ± 30	257 ± 8	6	-0.3 ± 0.4	-0.7 ± 0.7	-51.7	-51.1	257
North America	77 ± 17	72 ± 6	3	+0.9 ± 0.4	+1.5 ± 0.4	-51.3	-50.9	72
Europe	77 ± 15	80 ± 7	5	-0.4 ± 0.3	-1.1 ± 0.2	-52.3	-51.2	80
North Asia	110 ± 20	104 ± 10	8	+0.2 ± 0.4	-1.0 ± 0.7	-52.5	-51.1	104
Tropics	165 ± 20	195 ± 11	15	-0.9 ± 0.8	-0.9 ± 0.8	-51.8	-50.4	212
South America	35 ± 10	40 ± 7	14	-0.6 ± 0.7	-0.2 ± 0.1	-48.0	-43.3	39
Africa	56 ± 13	85 ± 9	7	+0.5 ± 0.3	-0.9 ± 0.4	-51.2	-49.5	105
Asia	74 ± 10	69 ± 8	4	-1.2 ± 0.5	+0.3 ± 0.4	-55.8	-55.4	68
SR	53 ± 15	53 ± 7	14	+1.4 ± 0.4	+0.1 ± 0.3	-54.6	-53.9	47
Ocean	15 ± 6	19 ± 6	2	+0.0 ± 0.3	+0.0 ± 0.3	-60.0	-60.0	18
<b>Growth rate</b>	<b>-12</b>	<b>19</b>						23
<b>Total sinks</b>	<b>509</b>	<b>506</b>						511
OH	484 ± 1	485 ± 1	<1**	+1.5	-0.5	-5.4*	-5.4*	485
Soils	25 ± 4	21 ± 3	15	+0.1 ± 0.1	+0.1 ± 0.1	-22.0	-21.9	26

Table A3: Methane budget for the 1984-2003 period. Estimates of sources and sinks of CH<sub>4</sub> for the period 1984-2003 (TgCH<sub>4</sub>/yr) presented either per source (process break), or per region (geographic break). Prior emissions are taken from EDGAR3 inventory<sup>9</sup> for anthropogenic sources and from inventories<sup>32, 33</sup> for natural emissions. Prior wetland emissions have been increased by a factor of 2 and prior landfills emissions have been increased by 50%. Biomass burning prior and spatio-temporal patterns are the mean of ref. 23. No inter-annual variability was considered in prior estimates of the emissions, except for ruminant animals. *Spread among ensemble members* represents the standard deviation of the results of the 18 inversions. *Decadal average rate of change in fluxes* is the long-term linear trend of each source calculated using a linear regression on annual means of the sources. Prior *Source  $\delta^{13}\text{C}$  signatures* were taken from ref. 18. For biomass burning, we accounted for the partition of C-3/C-4 plants<sup>22</sup> to evaluate one isotopic signature per region.

\*:For OH, we figure the kinetic isotopic fractionation. The last column gives the methane budget when adding an additional source due to plants (see text). \*\*:OH variability is prescribed from a methyl-chloroform inversion. Therefore, it is not optimized by the inversion. Uncertainties are one standard deviation.

## References

1. Dlugokencky, E. J., Houweling, S., Bruhwiler, L., Masarie, K. A. et al. Atmospheric methane levels off: Temporary pause or a new steady-state? *Geophys. Res. Lett.*, **30**, 1992, doi:10.1029/2003GL018126 (2003).
2. Gurney, K. R., Law, R. M., Denning, A. S., Rayner, P. J. et al. Towards robust regional estimates of CO<sub>2</sub> sources and sinks using atmospheric transport models. *Nature*, **415**, 626-630 (2002).
3. Bousquet, P., Hauglustaine, D. A., Peylin, P., Carouge, C. & Ciais, P. Two decades of OH variability as inferred by an inversion of atmospheric transport and chemistry of methyl chloroform. *Atmos Chem Phys*, **5**, 2635-2656 (2005).
4. Prinn, R. G., Huang, J., Weiss, R. F., Cunnold, D. M. et al. Evidence for substantial variations of atmospheric hydroxyl radicals in the past two decades (vol 292, pg 1882, 2001). *Science*, **293**, 1048-1048 (2001).
5. Dentener, F., Peters, W., Krol, M., van Weele, M. et al. Interannual variability and trend of CH<sub>4</sub> lifetime as a measure for OH changes in the 1979-1993 time period. *J. Geophys. Res.-atmos.*, **108**, 4442, doi:10.1029/2002JD002916 (2003).
6. Krol, M. & Lelieveld, J. Can the variability in tropospheric OH be deduced from measurements of 1,1,1-trichloroethane (methyl chloroform)? *J. Geophys. Res.-atmos.*, **108**, 4125, doi:10.1029/2002JD002423 (2003).
7. Hauglustaine, D. A., Hourdin, F., Jourdain, L., Filiberti, M. A. et al. Interactive chemistry in the Laboratoire de Meteorologie Dynamique general circulation model: Description and background tropospheric chemistry evaluation. *J. Geophys. Res.-atmos.*, **109**, D04314, doi:10.1029/2003JD003957 (2004).
8. Kaminski, T., Rayner, P. J., Heimann, M. & Enting, I. G. On aggregation errors in atmospheric transport inversions. *J. Geophys. Res.-atmos.*, **106**, 4703-4715 (2001).

9. Olivier, J. G. J. & Berdowski, J. J. M. in *The Climate System*, (eds. J. Berdowski, R. Guichert & B. Heij) p. 33–37 (2001).
10. FAO. (FAO, [www.fao.org](http://www.fao.org), 2005).
11. Peylin, P., Baker, D., Sarmiento, J., Ciais, P. & Bousquet, P. Influence of transport uncertainty on annual mean and seasonal inversions of atmospheric CO<sub>2</sub> data. *J. Geophys. Res.-atmos.*, **107**, - (2002).
12. GLOBALVIEW-CH4. Cooperative Atmospheric Data Integration Project - Methane. CD-ROM, NOAA CMDL [Also available on Internet via anonymous FTP to <ftp.cmdl.noaa.gov>, Path: [ccg/ch4/GLOBALVIEW](ftp://ccg/ch4/GLOBALVIEW)]. (2005).
13. Rodenbeck, C., Houweling, S., Gloor, M. & Heimann, M. CO<sub>2</sub> flux history 1982-2001 inferred from atmospheric data using a global inversion of atmospheric transport. *Atmos Chem Phys*, **3**, 1919-1964 (2003).
14. Miller, J. B., Mack, K. A., Dissly, R., White, J. W. C. et al. Development of analytical methods and measurements of C-13/C-12 in atmospheric CH<sub>4</sub> from the NOAA Climate Monitoring and Diagnostics Laboratory global air sampling network. *J. Geophys. Res.-atmos.*, **107**, 107, doi:10.1029/2001JD000630 (2002).
15. Quay, P., Stutsman, J., Wilbur, D., Snover, A. et al. The isotopic composition of atmospheric methane. *Global. Biogeochem. Cycles*, **13**, 445-461 (1999).
16. Thoning, K. W., Tans, P. P. & Komhyr, W. D. Atmospheric carbon dioxide at Mauna Loa Observatory. 2. Analysis of the NOAA GMCC data, 1974,1985. *J. Geophys. Res.*, **94**, 8549-8565 (1989).
17. Tyler, S. C., Ajie, H. O., Gupta, M. L., Cicerone, R. J. et al. Stable carbon isotopic composition of atmospheric methane: A comparison of surface level and free tropospheric air. *J. Geophys. Res.-atmos.*, **104**, 13895-13910 (1999).
18. Mikaloff Fletcher, S. E. M., Tans, P. P., Bruhwiler, L. M., Miller, J. B. & Heimann, M. CH<sub>4</sub> sources estimated from atmospheric observations of CH<sub>4</sub> and its C-13/C-12 isotopic ratios:

2. Inverse modeling of CH<sub>4</sub> fluxes from geographical regions. *Global. Biogeochem. Cycles*, **18**, GB4005, doi:10.1029/2004GB002224 (2004).
19. Houweling, S., Kaminski, T., Dentener, F., Lelieveld, J. & Heimann, M. Inverse modelling of methane sources and sinks using the adjoint of a global transport model. *Journal of Geophys. Research*, **104**, 26137-26160 (1999).
20. Wang, J. S., Logan, J. A., McElroy, M. B., Duncan, B. N. et al. A 3-D model analysis of the slowdown and interannual variability in the methane growth rate from 1988 to 1997. *Global. Biogeochem. Cycles*, **18**, 3011, doi:10.1029/2003GB002180 (2004).
21. Mikaloff Fletcher, S. E. M., Tans, P. P., Bruhwiler, L. M., Miller, J. B. & Heimann, M. CH<sub>4</sub> sources estimated from atmospheric observations of CH<sub>4</sub> and its C-13/C-12 isotopic ratios: 1. Inverse modeling of source processes. *Global. Biogeochem. Cycles*, **18**, GB4004, doi:10.1029/2004GB002223 (2004).
22. Van der Werf, G. R., Randerson, J. T., Collatz, G. J., Giglio, L. et al. Continental-scale partitioning of fire emissions during the 1997 to 2001 El Nino/La Nina period. *Science*, **303**, 73-76 (2004).
23. Van der Werf, G. R., Randerson, J. T., Collatz, G. J. & Giglio, L. Carbon emissions from fires in tropical and subtropical ecosystems. *Glob Change Biol*, **9**, 547-562 (2003).
24. Langenfelds, R. L., Francey, R. J., Pak, B. C., Steele, L. P. et al. Interannual growth rate variations of atmospheric CO<sub>2</sub> and its delta C-13, H-2, CH<sub>4</sub>, and CO between 1992 and 1999 linked to biomass burning. *Global. Biogeochem. Cycles*, **16**, 1048, doi:10.1029/2001GB001466 (2002).
25. Prigent, C., Matthews, E., Aires, F. & Rossow, W. B. Remote sensing of global wetland dynamics with multiple satellite data sets. *Geophys. Res. Lett.*, **28**, 4631-4634, doi:10.1029/2001GL013263 (2001).
26. Fung, I., John, J., Lerner, J., Matthews, E. et al. Three-dimensional model synthesis of global methane cycle. *J. Geophys. Res.*, **96**, 13033-13065 (1991).

27. Thornwaite, C. W. An approach towards a rational classification of climate. *Geogr. Rev.*, **38**, 55-89 (1948).
28. Uppala, S. M., Koallberg, P. W., Simmons, A. J., U. Andrae et al. The ERA-40 Reanalysis. *J. Roy. Met. Soc.*, **131**, 2961-3012 (2005).
29. Keppler, F., Hamilton, J. T. G., Braß, M. & Rockmann, T. Methane emissions from terrestrial plants under aerobic conditions. *Nature*, **439**, 187-191 (2006).
30. Krinner, G., Viovy, N., de Noblet-Ducoudre, N., Ogee, J. et al. A dynamic global vegetation model for studies of the coupled atmosphere-biosphere system. *Global. Biogeochem. Cycles*, **19**, GB1015, doi:10.1029/2003GB002199 (2005).
31. Prinn, R. G., Huang, J., Weiss, R. F., Cunnold, D. M. et al. Evidence for variability of atmospheric hydroxyl radicals over the past quarter century. *Geophys. Res. Lett.*, **32**, L07809, doi:10.1029/2004GL022228 (2005).
32. Matthews, E. & Fung, I. Methane emissions from natural wetlands, global distribution, area and environmental characteristics of sources. *Global. Biogeochem. Cycles*, **1**, 61-86 (1987).
33. Matthews, E. & Fung, I. Methane emissions from rice cultivation: geographic and seasonal distribution of cultivated areas and emissions. *Global. Biogeochem. Cycles*, **5**, 3-24 (1991).